Monthly Notices of the ROYAL ASTRONOMICAL SOCIETY

MNRAS **450,** 3472–3489 (2015) doi:10.1093/mnras/stv816

Galactic magnetic fields and hierarchical galaxy formation

L. F. S. Rodrigues,[1]★ A. Shukurov,[1] A. Fletcher[1] and C. M. Baugh[2]

[1]*School of Mathematics and Statistics, University of Newcastle, Newcastle upon Tyne NE1 7RU, UK*
[2]*Institute for Computational Cosmology, Department of Physics, University of Durham, South Road, Durham DH1 3LE, UK*

Accepted 2015 April 9. Received 2015 April 9; in original form 2015 January 4

ABSTRACT

A framework is introduced for coupling the evolution of galactic magnetic fields sustained by the mean-field dynamo with the formation and evolution of galaxies in cold dark matter cosmology. Estimates of the steady-state strength of the large-scale and turbulent magnetic fields from mean-field and fluctuation dynamo models are used together with galaxy properties predicted by semi-analytic models of galaxy formation for a population of spiral galaxies. We find that the field strength is mostly controlled by the evolving gas content of the galaxies. Thus, because of the differences in the implementation of the star formation law, feedback from supernovae and ram-pressure stripping, each of the galaxy formation models considered predicts a distribution of field strengths with unique features. The most prominent of them is the difference in typical magnetic field strengths obtained for the satellite and central galaxy populations as well as the typical strength of the large-scale magnetic field in galaxies of different mass.

Key words: galaxies: evolution – galaxies: magnetic fields.

1 INTRODUCTION

Magnetic fields have been detected in all spiral galaxies when observed at sufficient sensitivity and resolution (Beck et al. 1996; Beck & Wielebinski 2013). The most informative observational tracers of magnetic fields are partially polarized synchrotron emission and Faraday rotation. Polarized radio emission, together with significant Faraday rotation, indicate the presence of a component of the galactic magnetic field ordered on scales comparable to the resolution of the observation, of the order of a few hundred parsecs for nearby galaxies, and exceeding the integral turbulent scale which is of the order of 50–100 pc. The random (turbulent) magnetic field $\boldsymbol{b}$ is usually stronger than the large-scale component $\overline{\boldsymbol{B}}$, so the degree of polarization does not typically exceed 10–20 per cent. An average total field strength in nearby galaxies is $B = (\overline{B}^2 + b^2)^{1/2} \approx 9$ μG with $b/\overline{B} \simeq 1$–3 (Beck et al. 1996), ranging from about 4 μG in M31 (Fletcher et al. 2004) to 15μG in M51 (Fletcher et al. 2011).

Magnetic fields contribute significantly to the structure and evolution of the interstellar medium (ISM) and the host galaxy. They affect the accretion of gas by dark matter (DM) haloes (Rodrigues, de Souza & Opher 2010), as well as the outflows and inflows in galaxies that have already formed (Birnboim 2009). Magnetic fields also influence outflows since they affect the multiphase structure of the interstellar gas as they confine hot gas bubbles produced by supernovae (SNe; Ferriere, Mac Low & Zweibel 1991; Korpi et al. 1999; Shukurov et al. 2004; Hanayama & Tomisaka 2006). The magnetic contribution to the overall structure of galactic gas discs is at least as important as that from other sources of interstellar pressure, i.e. thermal, turbulent and from cosmic rays, as all of them are of comparable magnitude (Parker 1979; Bloemen 1987; Boulares & Cox 1990; Fletcher & Shukurov 2001). Half of the total interstellar pressure is thus due to non-thermal contributions, and, hence, magnetic fields directly affect the mean gas density. In turn, this affects significantly the star formation rate (SFR); it is perhaps surprising that the role of magnetic fields and cosmic rays in galaxy evolution has avoided attention for so long (Birnboim, Balberg & Teyssier 2015). Magnetic fields also regulate star formation locally by controlling the collapse and fragmentation of molecular clouds (Mac Low 2009; Peters et al. 2011; Crutcher 2012). Magnetic fields contribute to interstellar gas dynamics not only directly but also by confining cosmic rays (Berezinskii et al. 1990). The latter are effectively weightless and so are capable of driving galactic outflows (winds and fountains; Breitschwerdt & Komossa 2000; Everett et al. 2008; Uhlig et al. 2012; Booth et al. 2013) thus providing negative feedback on star formation in galactic discs (Veilleux, Cecil & Bland-Hawthorn 2005; Putman, Peek & Joung 2012).

Future radio telescopes such as the Square Kilometre Array[1] will allow a dramatic increase in the sensitivity and angular resolution of radio observations to permit not only detailed studies of nearby galaxies but also reliable and extensive measurements of galactic magnetic fields at higher redshifts (Gaensler, Beck & Feretti 2004). As we demonstrate here, the evolution of galactic magnetic fields

★ E-mail: luiz.rodrigues@newcastle.ac.uk

[1] http://www.skatelescope.org

is sensitive to a variety of poorly constrained parameters in galactic evolution models and can thus provide a sensitive diagnostic of the physical processes involved in galaxy formation.

The most successful theory for the production of magnetic fields observed in galaxies is the turbulent dynamo (for reviews, see Beck et al. 1996; Shukurov 2007). Two types of dynamo are expected to be important: the fluctuation dynamo, which produces a small-scale, random magnetic field of coherence lengths comparable to the turbulent scale in the plasma, and the mean-field dynamo, which produces a large-scale magnetic field ordered on scales greater than the turbulent scale. The details of the two dynamos are briefly discussed in Section 3.

There have been several attempts to understand the behaviour of large-scale magnetic fields in an evolving galaxy but they have been limited by the quality of galactic formation and evolution models available. Beck et al. (1994) suggested that the seed magnetic field for the large-scale dynamo can be produced in a protogalaxy or young galaxy by the fluctuation dynamo acting on a short timescale (see also Kulsrud et al. 1997; Arshakian et al. 2009; Schleicher et al. 2010; Sur et al. 2012; Seifried, Banerjee & Schleicher 2014), and thus the observed galactic magnetic fields can be generated in 1–2 Gyr for typical galactic properties. The seed magnetic field for the fluctuation dynamo can be produced by many mechanisms (Durrer & Neronov 2013) such as battery effects in the first generation of stars (Hanayama et al. 2005) or in a rotating protogalaxy (Mishustin & Ruzmaĭkin 1972).

The only evolutionary effect included by Beck et al. (1994) is a variation of the thickness of the galactic ionized gas layer with time. Arshakian et al. (2009, 2011) discuss dynamo action at various stages of galaxy formation at a qualitative level with reference to more recent models of galaxy formation and evolution.

Here, we quantitatively model the large-scale galactic magnetic fields produced by a mean-field dynamo in the framework of specific hierarchical galaxy formation models, with the aim of predicting the statistical properties of galactic magnetic fields in a large sample of galaxies at different redshifts. We employ semi-analytic models (SAMs) of galaxy formation based on simple physical prescriptions (for a review, see Baugh 2006). These models produce synthetic catalogues of galaxies that are able to reproduce a wide range of observables (e.g. the galaxy luminosity and stellar mass functions). Starting from the stellar and gaseous masses, disc sizes, SFRs and circular velocities, obtained from SAMs for late-type galaxies, we calculate magnetic fields using dynamo theory. The galaxy formation models remain uncertain regarding the details of the physical processes involved and their relative importance. In particular, the nature and intensity of the feedback of star formation on the galactic discs, which is in turn sensitive to the form and strength of the interstellar magnetic field, remains unclear.

We derive the dependence of the strength of magnetic field on the galactic mass, its evolution with redshift and the statistical distribution of magnetic field strengths in galactic samples. Remarkably, different SAMs lead to distinct predictions regarding galactic magnetic fields. Thus, magnetic fields observed in high-redshift galaxies via their polarization and Faraday rotation can help to refine galaxy formation models.

An alternative approach to galaxy formation and evolution in a cosmological context involves the numerical solution of the magnetohydrodynamic (MHD) equations for interstellar gas in the (evolving or static) gravity field obtained from N-body simulations. Gas dynamics is often simulated with adaptive mesh refinement (or a particle-based technique such as smooth particle hydrodynamics) in order to achieve higher spatial resolution in denser regions. In the best MHD simulations available now, the highest resolution is 20–300 pc (Wang & Abel 2009; Pakmor, Marinacci & Springel 2014). The driving of interstellar turbulence by SNe is neglected or parametrized. Moreover, the turbulent dynamo action responsible for both large-scale and turbulent interstellar magnetic fields obviously needs a fully resolved turbulent flow to be modelled accurately. As a result, the processes responsible for the large-scale magnetic field cannot be captured at all, and the simpler fluctuation dynamo is controlled by random flows at unrealistic scales. Even so, such results should be treated with care as turbulent magnetic fields are known to be sensitive to flows well within the inertial range of interstellar turbulence at scales of a fraction of parsec (Brandenburg & Subramanian 2005). Thus, MHD simulations of galaxy formation and evolution need to be complemented with SAMs coupled with a mean-field description of the large-scale magnetic field and models of the turbulent fields. The advantages of this approach include the opportunity to explore the parameter space and clarify the role of various physical effects. This opportunity is particularly attractive given that many important physical processes are already heavily parametrized in the hydrodynamic and MHD models.

The paper is organized as follows. In Section 2, we discuss SAMs of galaxy formation and evolution and Section 3 describes the generation of galactic magnetic fields by dynamo mechanisms. Our results for the distribution and evolution of galactic magnetic fields can be found in Section 4, together with a discussion on the systematic connection between the gas content of galaxies and magnetic fields, the role of magnetic helicity diffusion, the redshift evolution of galactic magnetic fields emerging from our models and the dependence of magnetic field on the SFR. Our conclusions are presented in Section 5. The appendices provide further details of the models.

2 GALACTIC EVOLUTION

To obtain the galaxy properties needed to compute the strength of galactic magnetic fields, we use SAMs of galaxy formation. These break down galaxy formation and evolution into a set of differential equations, each of which models a separate physical process, including: the merger history of DM haloes; the radiative cooling of gas inside these haloes and the subsequent formation of galactic discs; star formation in galactic discs; galaxy mergers driven by dynamical friction and bursts of star formation associated with them; the feedback due to SNe and AGNs and the chemical enrichment of stars and gas. (For reviews on these topics, see Baugh 2006; Benson 2010.)

We use three versions of the Durham SAM, GALFORM (Cole et al. 2000; Bower et al. 2006), the version presented by Baugh et al. (2005), hereafter referred to as BAU, that of Lagos et al. (2012), referred to as LAG and that of Font et al. (2008), hereafter FON. All models reproduce the galactic luminosity function at redshift $z = 0$ in the K and b_J bands. The BAU version of GALFORM successfully reproduces the counts and redshift distribution of galaxies selected according to their sub-millimetre luminosity, and the abundances of Lyman-break galaxies (Lacey et al. 2011) and Lyman α emitters (Orsi et al. 2008). The FON version provides a better match to the observed colours of satellite galaxies. The LAG version reproduces the atomic and molecular hydrogen mass functions (Lagos et al. 2011b), the K-band luminosity function at redshifts $z = 1$ and 2 (Lagos et al. 2011a) and the CO(1–0) luminosity function. Both LAG and FON are derived from the model of Bower et al. (2006) and predict the properties of the AGN population (Fanidakis et al. 2011, 2012).

The choice of these models allows us to assess the variability of the predictions between state-of-art SAMs and the impact of these differences on the galactic magnetic fields inferred from them.

2.1 Semi-analytic models of galaxy formation and evolution

The SAMs explored differ in various aspects, briefly described here. Further details can be found in the original papers referred to in the previous section.

2.1.1 Cosmological model and dark matter merger trees

The models differ in their assumed cosmologies and DM merger trees. The BAU model adopts a present-day cosmological constant energy density parameter $\Omega_\lambda = 0.7$, a matter density parameter $\Omega_m = 0.3$, a Hubble parameter $h = 0.7$ and a spectrum normalization $\sigma_8 = 0.93$. The LAG and FON models adopt the cosmological parameters of the Millennium Simulation (Springel et al. 2005), $\Omega_\lambda = 0.75$, $\Omega_m = 0.25$, $h = 0.73$ and $\sigma_8 = 93$.

The DM merger trees used in the LAG and FON models are extracted from the Millennium *N*-body cosmological simulation (Springel et al. 2005), which has a halo mass resolution of $1.72 \times 10^{10}\, h^{-1}\, M_\odot$. In the BAU model, the merger trees are built using the Monte Carlo procedure described by Cole et al. (2000), with the minimum final halo mass for the merger trees at $z = 0$ set to $5 \times 10^9\, h^{-1}\, M_\odot$.

2.1.2 Star formation and initial mass function

The models differ in their treatment of star formation in galaxy discs (quiescent star formation). In the BAU model, the galactic SFR is calculated as the ratio of the total mass of cold gas to the characteristic star formation time-scale, SFR $= M_g/\tau_\star$, with

$$\tau_\star = \tau_{\star 0} \left(\frac{V_0}{200\,\mathrm{km\,s^{-1}}} \right)^{\alpha_\star}, \quad (1)$$

where V_0 is the circular velocity at the half-mass radius of the disc, $\tau_{\star 0} = 8$ Gyr and $\alpha_\star = -3$. This prescription reproduces the observed gas fraction–luminosity relation at $z = 0$.

In the FON model, the star formation time-scale uses the parametrization

$$\tau_\star = \frac{\tau_{\mathrm{disc}}}{\epsilon_\star} \left(\frac{V_0}{200\,\mathrm{km\,s^{-1}}} \right)^{\alpha_\star}, \quad (2)$$

where $\tau_{\mathrm{disc}} = r_0/V_0$ is the disc dynamical time-scale and the free parameters $\epsilon_\star = 0.0029$ and $\alpha_\star = -1.5$ were chosen mainly to reproduce the galaxy luminosity function at $z = 0$ (Bower et al. 2006).

In the LAG model, the SFR per unit area is assumed to be proportional to the surface density of molecular hydrogen in the galactic disc. The amount of H_2 is obtained from the empirical relation of Blitz & Rosolowsky (2006) which relates the fraction of molecular hydrogen to the pressure in the mid-plane of the galactic disc.

The star formation prescription used in LAG has no free parameters in the sense that they are calibrated against observations of SFRs and gas surface densities in nearby galaxies. The parameters are in effect measured and are only allowed to span a narrow range of values consistent with observational errors, narrower than the ranges within which other model parameters are typically allowed to vary.

The stellar initial mass function (IMF) is assumed to be universal in LAG and FON, of the form proposed by Kennicutt (1983). BAU also assumes the Kennicutt IMF for quiescent star formation, but a top-heavy IMF is used for the starbursts.

2.1.3 Starbursts

In all models, galaxy mergers can trigger bursts of star formation, which transfer gas (and possibly stars) from the disc to the spheroidal component, where this gas participates in star formation. The merger events are instantaneous in the models and lead to either an elliptical galaxy (for a merger of galaxies of similar masses) or to a corresponding increase in the galaxy mass if the merging satellite galaxy has a mass much smaller than the central galaxy.

In LAG and FON, material is transferred to the spheroidal component, triggering a starburst also in the case when the galactic disc becomes dynamically unstable according to the bar stability criterion of Efstathiou, Lake & Negroponte (1982). The BAU model does not allow for any disc instabilities.

2.1.4 Stellar and AGN feedback

The models adopt similar parametrizations of the outflow due to SNe and stellar winds, with a mass-loss rate from the disc that depends on the SFR (a measure of the energy input into the ISM) and some power of the circular velocity of the disc (a measure of the depth of the potential well). The mass expelled is reincorporated into the disc at a later time. In the BAU model, this happens once the DM halo has doubled its mass, whereas in LAG and in FON, this occurs after a time $t = t_{\mathrm{dyn}}/\alpha_{\mathrm{rh}}$, where $t_{\mathrm{dyn}} = r_{\mathrm{virial}}/V_{\mathrm{virial}}$ is the dynamical time of the halo and $\alpha_{\mathrm{rh}} = 1.26$.

On the other hand, the models differ significantly in their assumptions about the processes that regulate the bright end of the galactic luminosity function. In BAU, galactic superwinds are assumed to eject material from haloes that have low circular velocity (with no subsequent reincorporation), at a rate proportional to the SFR. This reduces the baryon fraction in more massive haloes, which themselves are not directly subject to superwinds, thereby reducing the rate at which gas cools in these haloes. In LAG and FON, the growth of supermassive black holes in the centre of the galaxies is modelled and associated with an AGN feedback contribution. The cooling flow is interrupted once the black hole's Eddington luminosity exceeds a multiple of the cooling luminosity.

2.1.5 Ram-pressure stripping

When a galaxy becomes a satellite galaxy (after the merger of DM haloes), it loses part or all of its hot gas halo to the central system by ram-pressure stripping.

In BAU and LAG, this is modelled by transferring all of the hot gas halo of the satellite to the central galaxy, i.e. one assumes that the hot gas is completely and instantaneously stripped. In the FON, ram-pressure stripping is modelled more accurately, without assuming the instantaneous stripping of the gas. Instead, the prescription obtained from hydrodynamical simulations of McCarthy et al. (2008) is followed.

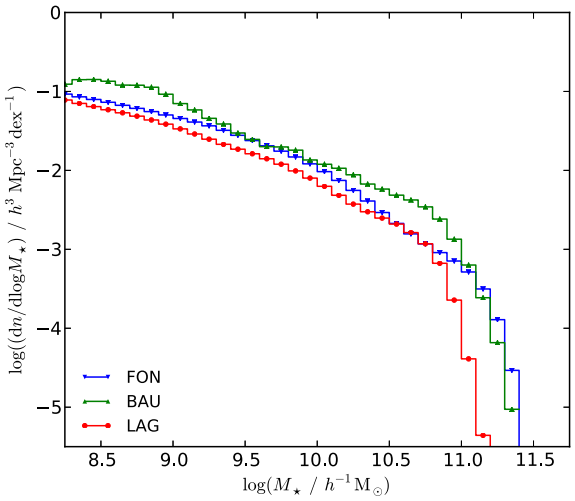

Figure 1. The late-type galaxy stellar mass function of the SAMs used. Different colours correspond to different SAMs as labelled.

2.2 Late-type galaxies and their properties

Magnetic fields ordered at the galactic scale only occur in late-type galaxies (since they have significant rotation), so we focus on these galaxies in what follows. We classify a galaxy as late type if its bulge stellar mass accounts for less than half the total galaxy mass.

Details of the galaxy formation models affect the distribution of galaxy stellar masses. In Fig. 1, this is shown for models explored.

2.2.1 Interstellar turbulence

Interstellar gas is vigorously driven into a turbulent state by the injection of kinetic energy, mostly from SN explosions (a general consequence of star formation), but also from stellar winds and other, less important sources (Elmegreen & Scalo 2004; Mac Low & Klessen 2004; Scalo & Elmegreen 2004). The root-mean-square (rms) turbulent speed is close to the sound speed in the warm gas ($T \simeq 10^4$–10^5 K) at $v_0 \simeq 10\,\mathrm{km\,s^{-1}}$ and exhibits weak variations within and between spiral galaxies (Tamburro et al. 2009). The turbulent scale $l_0 \simeq 0.1$ kpc is controlled by the size of an SN remnant when its expansion velocity decreases to the sound speed in the ambient warm gas: the expanding SN shell drives flows in its wider environment only from this stage onwards.

The small variability in the turbulent speed may seem surprising as one might expect a dependence of v_0 on the SFR. Indeed, detections of such a dependence through H I observations have been reported (Dib, Bell & Burkert 2006). However, both the interpretation of such observations and the connection between SFR and turbulence are far from straightforward. Apart from driving turbulent motions, SN activity is responsible for the hot phase of the interstellar gas, and the filling factor of the hot phase increases with SFR (de Avillez & Breitschwerdt 2004). The energy released by SNe is distributed among several such channels (including radiative cooling, acceleration of cosmic rays, etc.), and it is not obvious that an enhanced SFR would necessarily lead to a larger turbulent velocity. The fact that the turbulence observed in the warm interstellar gas is transonic is likely not to be a coincidence, but rather a result of non-linear feedback between star formation and turbulence. If the turbulent driving becomes stronger because of an increase in the SFR, the turbulence initially becomes supersonic, leading to a rapid dissipation of kinetic energy into heat in the shocks, so that the turbulent kinetic energy is reduced, being converted into thermal energy of the warm gas (the speed of sound in the hot gas is of the order of $100\,\mathrm{km\,s^{-1}}$, so the warm gas absorbs most of the extra kinetic energy). As a result, the gas temperature increases until the turbulence becomes transonic and the system reaches a new (quasi-)steady state. However, the gas cools radiatively, on a cooling time-scale (of a few 10^3 yr for temperatures near 10^4 K, assuming solar metallicity) that is shorter than the typical time-scale of variations in the SFR (of the order of 10^6 yr). Thus, the warm gas can adjust itself to the varying SFR remaining at a nearly constant equilibrium temperature of $T = 10^4$–10^5 K which is known to be rather insensitive to the heating rate because of the efficient cooling. As a result, the extra energy supplied by the SNe is more plausibly lost as radiation and, more importantly here, increases the fractional volume of the hot gas. This enhances the associated outflow from the gas disc but does not increase the turbulent velocity. In other words, the turbulent velocity in the warm gas is controlled by its sound speed, i.e. by the balance of heating and cooling which, ultimately, is determined by its chemical composition (the metal abundance).

Outflows (fountains or winds) driven by SN activity entrain significant amounts of warm and cold gas (e.g. Gent et al. 2013b; McCourt et al. 2015), so it is not surprising that observations at a relatively low resolution (1 kpc or larger) can pick up a broad range of velocities dominated by outflows rather than the turbulent motions in the warm gas.

To conclude, we keep the turbulent velocity and scale fixed and independent of the SFR at $v_0 = 10\,\mathrm{km\,s^{-1}}$ and $l_0 = 0.1$ kpc. However, the outflow speed is a sensitive function of the SFR in our model (Section 2.2.5).

2.2.2 Derived galactic quantities

The calculation of the magnetic field in a galaxy that is described in Section 3 requires knowledge of the average gas density, $\overline{\rho}$, and the average disc height, $\overline{h}$. In this section, we derive simple expressions for these two quantities as functions of galaxy properties output by SAMs (see Table 1 for a summary of the notation and quantities involved).

Assuming that the surface density of the disc of the galaxy is well described by an exponential profile, the height of a gaseous disc in hydrostatic equilibrium is given by (see Appendix A for a derivation)

$$h(r) = \frac{\alpha v_0^2 r_\mathrm{s}^2}{3\,G(M_\star + M_\mathrm{gas})}\,\mathrm{e}^{r/r_\mathrm{s}}\,, \tag{3}$$

where v_0 is the turbulent velocity of the disc gas, r_s is the radial scalelength of the disc and α is the number of pressure contributions to the support of the gaseous disc. We use $\alpha = 4$, assuming equal contributions from thermal, turbulent, cosmic ray and magnetic pressures.

Equation (3) leads to a divergent galaxy volume unless it is truncated. We choose the half-mass radius as the galactic boundary, $r_0 = \xi r_\mathrm{s}$ with $\xi \approx 1.678$, so that the volume of the galaxy follows as

$$V = 2\pi \int_0^{r_0} h(r) r\,\mathrm{d}r = 2\pi\lambda r_0^2 h(0)\,, \tag{4}$$

where

$$\lambda = \int_0^1 x\mathrm{e}^{\xi x}\,\mathrm{d}x \approx 1.645\,.$$

Table 1. Summary of the quantities used and notation.

Type of parameter	Notation	Meaning	Defined in or the value adopted
Galactic properties obtained from the semi-analytic models of galaxy formation	$M_{\rm g}$	Cold gas mass of a galaxy	
	$M_\star$	Stellar mass of a galaxy	
	$r_{50,\rm out}$	Half-mass radius of the galactic disc	
	V_0	Circular velocity of the galactic disc at the half-mass radius	
	SFR	Star formation rate in the disc	
Quantities estimated in this paper	$\overline{h}$	Average scaleheight of the galactic disc	Equation (5)
	$\overline{\rho}$	Average gas density in the galactic disc	Equation (7)
	r_0	Corrected half-mass disc radius	Equation (10)
	Ω	Angular velocity of the disc	Equation (11)
	S	Maximum rotational shear	Equation (12)
	$v_{\rm ad}$	Local outflow speed	Equation (19)
Adopted parameters	l_0	Characteristic length-scale of the turbulence	0.1 kpc
	v_0	Root-mean-square gas velocity dispersion in the disc	$10\,{\rm km\,s^{-1}}$
	α	Number of contributions to the interstellar pressure	4 (equation A6)
	R_κ	Ratio of turbulent diffusivities of the mean helicity and large-scale magnetic field	0.3 (equation 28)
Computed quantities	R_u	Outflow magnetic Reynolds number	Equation (27)
	D	Dynamo number	Equation (25)
	$D_{\rm c}$	Critical dynamo number	Equation (29)
	$\overline{B}$	Steady-state large-scale magnetic field strength	Equation (30)
	b	Steady-state random magnetic field strength	Equation (24)

The average disc scaleheight can be defined as

$$\overline{h} = \frac{V}{2\pi r_0^2} = \frac{\alpha v_0^2 r_0^2}{3G\left(M_\star + M_{\rm gas}\right)}\xi\,, \tag{5}$$

which yields

$$\overline{h} \simeq 287\,{\rm pc}\left(\frac{r_0}{10\,{\rm kpc}}\right)^2\left(\frac{v_0}{10\,{\rm km\,s^{-1}}}\right)^2 \times \frac{\alpha}{4}\left(\frac{M_\star + M_{\rm gas}}{10^{11}\,{\rm M_\odot}}\right)^{-1}. \tag{6}$$

The average gas density is then obtained as

$$\overline{\rho} = \frac{M_{\rm gas}}{2\,V} = \frac{GM_{\rm gas}(M_{\rm gas}+M_\star)}{\alpha v_0^2 r_0^4}\frac{3\xi^2}{4\pi\lambda}\,, \tag{7}$$

or

$$\overline{\rho} \simeq 1.06\times10^{-23}\,{\rm g\,cm^{-3}}\left(\frac{\alpha}{4}\right)^{-1}\left(\frac{r_0}{10\,{\rm kpc}}\right)^{-4} \times \left(\frac{M_{\rm gas}}{10^{10}\,{\rm M_\odot}}\right)\left(\frac{M_{\rm gas}+M_\star}{10^{11}\,{\rm M_\odot}}\right)\left(\frac{v_0}{10\,{\rm km\,s^{-1}}}\right)^{-2}. \tag{8}$$

The factor $1/2$ in equation (4) allows for the fact that r_0 in equation (4) is the half-mass radius, thus enclosing half of the total mass.

2.2.3 Disc size

Reproducing the observed sizes of galactic discs is a long-standing problem in SAMs of galaxy formation (e.g. González et al. 2009). Because of the strong dependence of the derived quantities on the disc size, we have renormalized the disc half-mass radii so that the medians of the predicted half-mass radii match the fit obtained by Dutton et al. (2011) for the observed relation between the half-mass radius and the stellar mass of SDSS galaxies at $z = 0$,

$$r_{50,\rm emp}(z=0) = r_D\left(\frac{M_\star}{M_D}\right)\left[\frac{1}{2}+\frac{1}{2}\left(\frac{M_\star}{M_D}\right)^{c_3}\right]^{(c_2-c_1)/c_3}, \tag{9}$$

where

$$(c_1, c_2, \log_{10} M_D, \log_{10} r_D, c_3) = (0.2, 0.46, 10.39, 0.75, 1.95)\,.$$

Thus, the corrected half-mass radius of a disc galaxy in a particular mass bin is related to the original disc size in the output of the SAM, $r_{50,\,\rm out}$ through

$$r_0(z) = r_{50,\rm out}(z)\frac{r_{50,\rm emp}(z=0)}{r_{50,\rm median}(z=0)}. \tag{10}$$

This procedure corrects the median values of the disc radii in each mass bin, preserving the dispersion of disc sizes predicted by the models and the redshift evolution of the mass–size relation. In Fig. 2, we show the original and corrected size–mass relations for each SAM.

2.2.4 Rotation and velocity shear

An estimate of the disc angular velocity, Ω, is necessary in the modelling of galactic magnetic fields. This is computed at the half-mass radius, r_0, using

$$\Omega = \Omega_0 = \frac{V_0}{r_0}\,, \tag{11}$$

where V_0 is the disc's circular velocity at $r = r_0$.

The next quantity to compute is the shear, $S = r\,\partial\Omega/\partial r$. We employ the maximum value of S in our calculations. It can be shown that the maximum shear in a purely exponential disc is related to the angular velocity through

$$S \approx -0.76\,\Omega_0\,. \tag{12}$$

2.2.5 Galactic outflows

The mean-field dynamo, responsible for the generation of a large-scale galactic magnetic field, relies on the removal of small-scale fields (and their magnetic helicity) away from the dynamo region

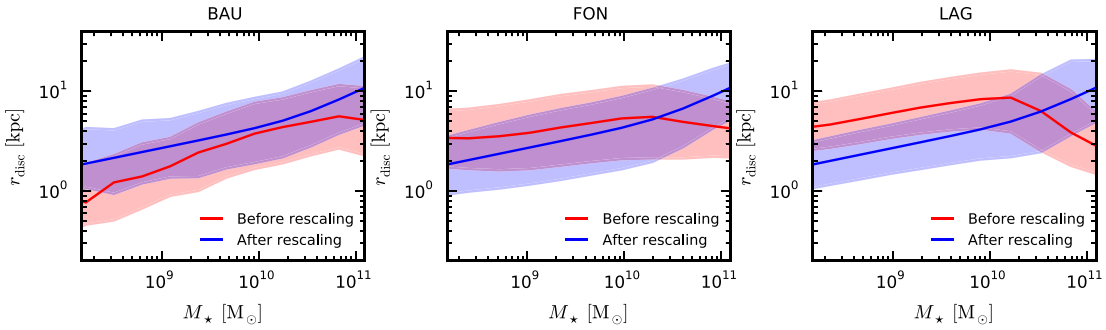

Figure 2. Disc size–stellar mass relation for the three SAMs used here. The red curves and corresponding shaded areas show to medians and the range between the 15th and 85th percentiles for the raw model output. The blue curves and corresponding shaded areas show the same data after the rescaling to make the medians match the fit to observational data given by equation (9). Each panel shows a different model as labelled.

in order to saturate in a steady state where the field has a strength comparable to that observed, of several microgauss (Brandenburg & Subramanian 2005). As discussed by Shukurov et al. (2006), in galaxies this can be achieved by the advection of magnetic fields by the outflow of the hot gas (and its entrained colder components) from the disc, as well as by turbulent diffusion (Kleeorin et al. 2000, and references therein).

While the SAMs have internal prescriptions to compute the amount of gas that outflows from the disc due to SNe-powered galactic winds, the gas carried by these winds is thought to be removed completely from the galaxy, and becomes available for reincorporation into the hot halo only after time-scales larger than dynamical time of the DM halo. These strong winds, however, correspond only to a fraction of the total outflow.

The outflow relevant for the magnetic field evolution is the one associated with galactic fountains, which leads to the removal of hot magnetized gas from the mid-plane of the disc but with a possibly very short re-accretion time-scale. This is not considered explicitly in the SAMs. We model this process as follows (see also Lagos, Lacey & Baugh 2013).

SNe tend to cluster in OB associations, regions of active star formation. The large, energetic bubbles of hot gas (superbubbles) produced by dozens of SNe and stellar winds in an OB association can more readily break out from the galactic disc. In the framework of the superbubble model of Mac Low & McCray (1988), the speed of the shock front at the top of an expanding superbubble at its break-out is given by (see Appendix B for derivation)

$$v_{\rm sh} = 4\,{\rm km\,s^{-1}} \left(\frac{n_0}{1\,{\rm cm^{-3}}}\right)^{-1/3} \left(\frac{h}{1\,{\rm kpc}}\right)^{-2/3}, \tag{13}$$

where n_0 is the mean number density of the gas in the disc. Note that we have assumed that the OB associations can be treated as identical (i.e. they share a common equivalent mechanical luminosity and the SN rate within them is approximately the same).

The interesting quantity, however, is the average of $v_{\rm sh}$ over the whole galaxy, $\overline{v}_{\rm sh}$, taking into account the *rate of occurrence* of OB associations. This can be estimated as follows:

$$\overline{v}_{\rm sh} = v_{\rm sh} \frac{A_{\rm OB}}{A_{\rm gal}}, \tag{14}$$

where $A_{\rm gal} = \pi r_0^2$ is the surface area of the galaxy. The total area filled with OB associations is

$$A_{\rm OB} = N_{\rm OB} \pi (2\,h)^2\,, \tag{15}$$

since the radius of an OB association at the break-out is about $2h$ (Mac Low & McCray 1988). The number of OB associations can be obtained from the frequency of SNe occurrence in OB associations, $\nu_{\rm SN,OB}$, and the rate of SNe occurrence in a single OB association,$\nu_{\rm SN,1OB}$,

$$N_{\rm OB} = \frac{\nu_{\rm SN,OB}}{\nu_{\rm SN,1OB}}\,. \tag{16}$$

The frequency of SN occurrence in OB associations is approximately 70 per cent of the total SN frequency Tenorio-Tagle & Bodenheimer (1988), i.e. $\nu_{\rm SN,OB} = f_{\rm OB}\nu_{\rm SN}$ with $f_{\rm OB} \approx 0.7$. The overall SNe frequency relates to the SFR through $\nu_{\rm SN} = \eta_{\rm SN} \times$ SFR, where $\eta_{\rm SN} = 9.4 \times 10^{-3}\,{\rm M_\odot^{-1}}$ for Kennicutt IMF (Kennicutt 1983).

The frequency of SNe within a single OB association can be found from the number of SNe that typically occur in one OB association, $N_{\rm SN,1OB} \approx 40$ (Heiles 1987), and the typical lifetime of an OB association is $t_{\rm OB} = 3 \times 10^6$ yr, i.e. $\nu_{\rm SN,1OB} \simeq t_{\rm OB}^{-1} N_{\rm SN,1OB}$. Thus, we find that the number of OB associations in a galaxy at a given epoch is related to its SFR through

$$N_{\rm OB} \approx 490 \left(\frac{\rm SFR}{\rm M_\odot\,yr^{-1}}\right) \left(\frac{N_{\rm SN,1OB}}{40}\right)^{-1} \times \left(\frac{t_{\rm OB}}{3\times10^{-3}\,{\rm Gyr}}\right) \left(\frac{f_{\rm OB}}{0.7}\right). \tag{17}$$

Using equations (13)–(17) one obtains

$$\overline{v}_{\rm sh} = 1.5\,{\rm km\,s^{-1}} \left(\frac{\rm SFR}{\rm M_\odot\,yr^{-1}}\right) \left(\frac{n_0}{1\,{\rm cm^{-3}}}\right)^{-1/3} \times \left(\frac{\overline{h}}{200\,{\rm pc}}\right)^{4/3} \left(\frac{r_0}{5\,{\rm kpc}}\right)^{-2}. \tag{18}$$

This is the gas speed in (and immediately behind) the shock front of a superbubble. At the time-scales involved, the magnetic field can be assumed to be frozen into the gas and thus is lost from the disc together with the gas. Therefore, the quantity of interest is the mass-averaged speed, $v_{\rm ad}$, such that the surface density of mass-loss from the disc is $\overline{\rho} v_{\rm ad}$:

$$v_{\rm ad} = \overline{v}_{\rm sh} \frac{\rho_{\rm h}}{\overline{\rho}}\,, \tag{19}$$

where $\rho_{\rm h} \approx 1.7 \times 10^{-27}\,{\rm g\,cm^{-3}}$ is the density of the hot gas and ρ is the average interstellar gas density.

3 MODELS OF GALACTIC MAGNETIC FIELDS

A partially ordered magnetic field $\boldsymbol{B}$ in the turbulent interstellar gas can be conveniently represented as the sum of a large-scale, $\overline{\boldsymbol{B}}$, and a fluctuating, $\boldsymbol{b}$, components,

$$\boldsymbol{B} = \overline{\boldsymbol{B}} + \boldsymbol{b}\,, \qquad \overline{\boldsymbol{b}} = \boldsymbol{0}\,,$$

where a bar denotes the ensemble or any other suitable average (see Gent et al. 2013a, for a discussion of averaging procedures).

The growth time of the large-scale magnetic field due to the mean-field turbulent dynamo (Moffatt 1978; Ruzmaikin, Shukurov & Sokoloff 1988) can be estimated as (Ji et al. 2014)

$$\tau_{\rm MF} \simeq 2\frac{h^2}{\eta}(D_{\rm c} - D)^{-1/2}\,, \quad |D| > |D_{\rm c}|\,, \tag{20}$$

where the magnetic diffusivity η, dominated by the turbulent contribution, is estimated from mixing-length theory as

$$\eta \simeq \frac{1}{3} l_0 v_0\,,$$

with l_0 and v_0 the turbulent scale and speed, respectively, the dynamo number D (that quantifies the strength of the dynamo action) can be written using equations (25) and (26) as

$$D \simeq \left(\frac{h l_0}{\eta}\right)^2 \Omega S\,,$$

with S being the rotational shear rate, and $D_{\rm c}$ is a critical value of the dynamo number such that magnetic field can be maintained only if $D < D_{\rm c}$ ($D < 0$ so long as Ω decreases with r). We note that h^2/η is the turbulent diffusion time across a layer of a scaleheight h. Equation (20) is quite accurate for the range of $|D|$ of interest in applications to spiral galaxies (see the discussion in Ji et al. 2014). For a flat rotation curve, $S = -\Omega$, and $|D| \gg |D_{\rm c}|$, which is true in the inner parts of most galaxies, we obtain $D \simeq -10(h\Omega/v_0)^2$ and

$$\tau_{\rm MF} \simeq \frac{2h}{l_0\Omega} \tag{21}$$

$$\simeq 4\times10^8\ {\rm yr}\left(\frac{h}{0.5\,{\rm kpc}}\right)\left(\frac{\Omega}{25\,{\rm km\,s^{-1}\,kpc^{-1}}}\right)^{-1}\left(\frac{l_0}{0.1\,{\rm kpc}}\right)^{-1}, \tag{22}$$

normalized to the parameter values corresponding to the solar vicinity of the Milky Way. In the inner parts of slowly rotating galaxies and in outer regions of normal disc galaxies, $\tau_{\rm MF}$ is shorter than the galactic evolution time-scale $\tau_{\rm e} \simeq 10^9$ yr.

Random magnetic fields grow even faster due to fluctuation dynamo action (note that this dynamo action is distinct from the more commonly discussed mean-field dynamo), on a time-scale shorter than the turnover time of the largest turbulent eddy, $\tau_0 \simeq l_0/v_0 \simeq 10^7$ yr.

The exponential growth on the time-scales specified above halts (the dynamo action is said to saturate) as soon as the Lorentz force becomes comparable to other forces on the relevant length-scale, of the order of 1 kpc, for the large-scale magnetic field and a fraction of the turbulent scale for the random field (Bhat & Subramanian 2013). After that, magnetic fields remains in a statistically steady state. The magnitudes of $\overline{\boldsymbol{B}}$ and $\boldsymbol{b}$ in this state are discussed further in this section. A recent review and a suite of formulae describing non-linear mean-field dynamos can be found in Chamandy et al. (2014).

Thus, as a first approximation, we can assume that: (i) galactic magnetic fields adjust themselves instantaneously to the evolving galactic environment (i.e. $\tau_{\rm MF}$, $\tau_0 \ll \tau_{\rm e}$) and (ii) they always remain in a statistically steady state of a saturated dynamo. These assumptions are obviously crude. However, they are sufficient for a first exploration of the effects of magnetic fields on galaxy evolution if the exploration then continues to include the effects of finite dynamo time-scales. The latter will be our subject elsewhere.

3.1 Random magnetic fields in spiral galaxies

Any random flow of electrically conducting fluid is a dynamo (i.e. it amplifies a seed magnetic field exponentially fast) provided the magnetic Reynolds number due to Ohmic magnetic diffusivity, $R_{\rm m} = l_0 v_0/\eta$, exceeds a certain critical value, $R_{\rm m,cr}$ of the order of 100 in an incompressible flow. This type of a dynamo is known as the *fluctuation dynamo* (Zeldovich, Ruzmaikin & Sokoloff 1990; Schekochihin et al. 2002b; Brandenburg & Subramanian 2005).

The growth time of the random magnetic field in a *vortical* random velocity field of a scale l is as short as the kinematic time at that scale, $\tau \simeq l/v(l)$ with $v(l)$ the rms random speed at the scale l. In a turbulent flow with a sufficiently shallow power spectrum, τ is shorter on smaller scales. For example, $\tau \propto l^{2/3}$ in a flow with the Kolmogorov spectrum $v(l) \propto l^{1/3}$. Therefore, the magnetic energy spectrum peaks at small scales during the exponential growth (kinematic) stage, and then plausibly settles to a form similar to that of the kinetic energy spectrum in the statistically steady state (a saturated, non-linear dynamo). The eddy turnover time in spiral galaxies, where $l_0 \simeq 0.1$ kpc and $v_0 \simeq 10\,{\rm km\,s^{-1}}$, is as short as $\tau_0 \simeq l_0/v_0 \simeq 10^7$ yr even at the energy scale of the interstellar turbulence. Thus, the fluctuation dynamo can rapidly produce random magnetic fields in the ISM (Shukurov 2007).

Compressibility hinders the fluctuation dynamo, reducing the growth rate of the random magnetic field. In the extreme case of sound-wave turbulence, the longitudinal nature of the fluid motions reduces the probability of three-dimensional twisting and folding of magnetic lines, an essential element of the amplification mechanism (as in Zeldovich's stretch–twist–fold dynamos – Zeldovich, Ruzmaikin & Sokoloff 1983; Zeldovich et al. 1990). As a result, the growth time of the rms magnetic field is of the order of $\tau \simeq \mathcal{M}^{-4} l_0/v_0$ for $\mathcal{M} \ll 1$, where $\mathcal{M}$ is the Mach number (Kazantsev, Ruzmaikin & Sokolov 1985). A generic compressible turbulence inherits this feature, producing a higher threshold value of $R_{\rm m}$ and slower growth of magnetic energy (Haugen, Brandenburg & Mee 2004; Federrath et al. 2011; Gent et al. 2013b). We note, however, that the velocity field in such flows is a mixture of solenoidal and compressible parts (Moss & Shukurov 1996), with their relative contributions depending on the Reynolds number, Mach number, numerical resolution, etc. (Haugen et al. 2004; Mee & Brandenburg 2006). Haugen et al. (2004) find, in their simulations of dynamo action in a compressible random flow, that $R_{\rm m,cr}$ increases from about 35 at $\mathcal{M} = 0$–60 at $\mathcal{M} = 1$ and 80 at $\mathcal{M} = 2.5$ (for the magnetic Prandtl number $P_{\rm m} = R_{\rm m}/{\rm Re} = 1$ with Re the Reynolds number) but suggest that $R_{\rm m,cr}$ may vary little as the Mach number increases further, especially for a large magnetic Prandtl number (as in the interstellar gas). Federrath et al. (2011) find $\tau \propto \mathcal{M}^{-1/3}$ for $10 < \mathcal{M} < 20$ in their simulations of isothermal compressible random flows.

However, slower growth and a higher dynamo threshold in a compressible random flow, as compared with incompressible flows, may not in fact represent a practical problem since the value of the magnetic Reynolds number is usually very high in astrophysical plasmas, and the turbulent kinematic time-scale l_0/v_0 is very short in comparison with any global time-scale in galaxies. What is more

important is the steady-state magnitude of the magnetic energy density relative to the kinetic energy density of turbulence. According to Federrath et al. (2011), isothermal compressible random flows produce lower magnetic energy density $E_{\rm m} = b^2/8\pi$ relative to the kinetic energy density $E_{\rm k} = \frac{1}{2}\rho v_0^2$, with $E_{\rm m}/E_{\rm k} \simeq 10^{-2}$–$10^{-3}$ at $2 < \mathcal{M} < 20$ than a purely solenoidal velocity field. Thus, gas compressibility is detrimental to the fluctuation dynamo in both the kinematic and saturated regimes.

The magnetic field produced by the fluctuation dynamo is intermittent, and can be described as a statistical ensemble of magnetic flux ropes and sheets whose coherence size (length or radius of curvature) is of the order of the flow correlation length, l_0, whereas the rope thickness is, in the kinematic dynamo, of the order of the resistive scale, $l_0 R_{\rm m}^{-1/2}$, (Zeldovich et al. 1990). Wilkin, Barenghi & Shukurov (2007) show that flux ropes become progressively dominant as $R_{\rm m}$ increases in the kinematic regime.

Kinematic fluctuation dynamos are well understood, but the non-linear, statistically steady state remains, to some extent, controversial. Simulations of fluctuation dynamos in driven random flows suggest that magnetic energy density within the ropes is close to equipartition with the kinetic energy density (Brandenburg & Subramanian 2005),

$$B_{\rm eq} = v_0 (4\pi\rho)^{1/2} . \tag{23}$$

A widely accepted model for the saturation of the fluctuation dynamo by Subramanian (1999, see also Subramanian, Shukurov & Haugen 2006), suggests that, in the steady state, the magnetic Reynolds number is renormalized to its critical value, so that the thickness of magnetic ropes is estimated as $d \simeq l_0 R_{\rm m,cr}^{-1/2} \simeq 0.1 l_0$ for $R_{\rm m,cr} = 100$ independently of $R_{\rm m}$ (see however, Schekochihin et al. 2002a). For modest effective magnetic Reynolds numbers, $R_{\rm m} \simeq R_{\rm m,cr}$, magnetic sheets may be predominant. Then the volume filling factor f_B of the magnetic structures can be estimated assuming that there is one magnetic sheet per correlation cell of the turbulent flow:

$$f_B = \frac{d}{l_0} \simeq R_{\rm m,cr}^{-1/2} \simeq 0.1,$$

so that the rms magnetic field follows as

$$b \simeq f_B B_{\rm eq} = f_B\, v_0 (4\pi\rho)^{1/2}. \tag{24}$$

However, magnetic field outside the dominant magnetic structures can still contribute significantly to the observables, such as the random Faraday rotation measure (Bhat & Subramanian 2013), so that this estimate should be applied judiciously.

3.2 Regular magnetic fields in spiral galaxies

The generation of large-scale magnetic fields in galaxies is described by galactic dynamo theory using the concept of a mean-field dynamo (see Beck et al. 1996; Shukurov 2007, for a review). Dynamo action in a rotating, stratified galactic gas layer is produced by the joint action of the helical turbulent motion (via the so-called α-effect) and the differential rotation of the galactic disc. These two effects are quantified, respectively, by two dimensionless parameters,

$$R_\alpha = \frac{\alpha_0 h}{\eta} \quad \text{and} \quad R_\omega = \frac{S h^2}{\eta} .$$

The widely used $\alpha\omega$-dynamo approximations applies where $|R_\omega| \gg R_\alpha$. In this approximation, dynamo action is controlled solely by their product, known as the dynamo number,

$$D = R_\alpha R_\omega . \tag{25}$$

The magnitude of the α-effect can be obtained from the order-of-magnitude estimate

$$\alpha_0 \simeq \frac{l_0^2 \Omega}{h} . \tag{26}$$

It is not quite clear how the mean-field dynamo enters a non-linear, steady state (for a review, see Brandenburg & Subramanian 2005). In the most detailed and physically motivated theory available, the growth of the large-scale magnetic field is limited by the conservation of magnetic helicity, so its steady-state strength depends on the rate at which the mean magnetic helicity of the random magnetic field is removed from the localization region of the large-scale magnetic field (Del Sordo, Guerrero & Brandenburg 2013). In galaxies, this can be accomplished by galactic winds and fountain flows (Shukurov et al. 2006; Sur, Shukurov & Subramanian 2007). In this case an additional dimensionless parameter enters the picture, quantifying the *advection* of magnetic helicity out of the galactic disc

$$R_u = \frac{v_{\rm ad} h}{\eta} . \tag{27}$$

Another mechanism that contributes to the partial removal of the small-scale magnetic helicity is its turbulent diffusion (Kleeorin et al. 2000, 2002, 2003). Allowing for this effect introduces another dimensionless number, the diffusivity ratio of the mean current helicity, κ, and the mean magnetic field, η:

$$R_\kappa = \frac{\kappa}{\eta} . \tag{28}$$

Mitra et al. (2010) obtained $R_\kappa \approx 0.3$ independent of the Reynolds number.

To summarize this model (see Chamandy et al. 2014, for details), a disc galaxy has an active mean-field dynamo (i.e. it is capable of amplifying and sustaining a large-scale magnetic field) if the magnitude of the dynamo number, equation (25), exceeds that of its critical value,

$$D_{\rm c} = -\left(\frac{\pi}{2}\right)^5 \left(1 + \frac{R_u}{\pi^2}\right)^2 . \tag{29}$$

For $|D| < |D_{\rm c}|$, the large-scale magnetic field decays on a time-scale of the order of h^2/η. Otherwise, $\overline{\boldsymbol{B}}$ is exponentially amplified up to the steady-state strength

$$\overline{B}^2 \simeq \frac{1}{2}\zeta(p) B_{\rm eq}^2 \left(\frac{l_0}{h}\right)^2 \left(\frac{D}{D_{\rm c}} - 1\right) \left(R_u + \pi^2 R_\kappa\right) , \tag{30}$$

where the magnetic pitch angle, defined as $p \equiv \arctan\left(\overline{B}_r/\overline{B}_\phi\right)$ in terms of the cylindrical magnetic field components, can be expressed in term of the previous quantities as

$$p = \arctan\left(\frac{1}{R_\omega}\left|\frac{2\,D_{\rm c}}{\pi^{1/2}}\right|\right) , \tag{31}$$

with $B_{\rm eq}$ defined in equation (23), and

$$\zeta(p) = \left(1 - \frac{3\sqrt{2}}{8}\cos^2 p\right)^{-1} . \tag{32}$$

4 RESULTS AND DISCUSSION

In this section, we identify and interpret robust features of galactic magnetic fields obtained from the galaxy formation models. Our results refer to statistical properties of large-scale and random magnetic fields in large samples of galaxies. We found that magnetic

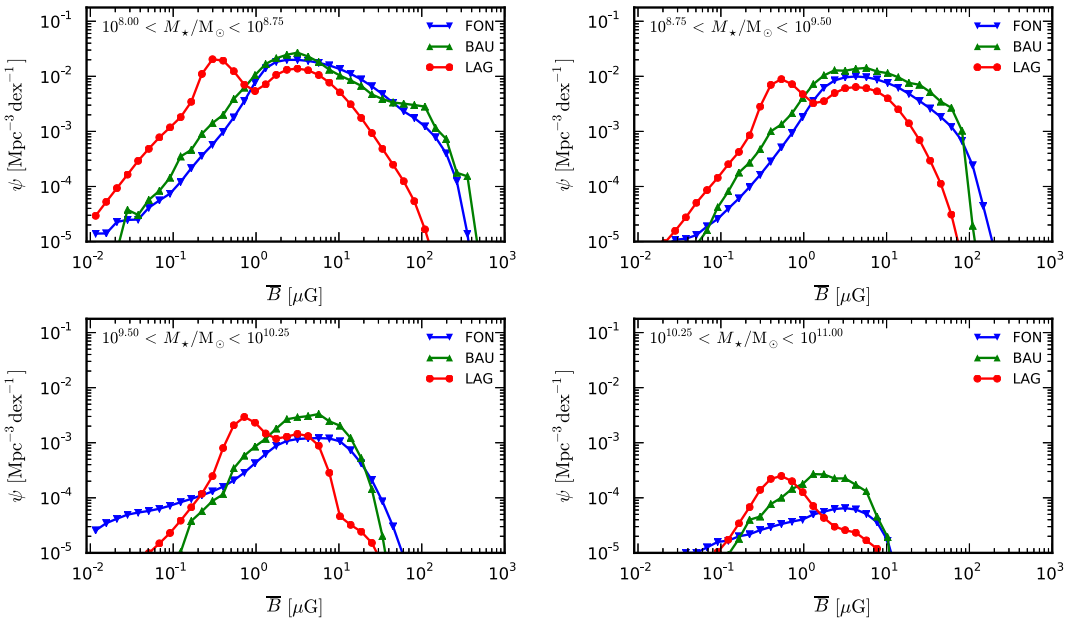

Figure 3. The predicted magnetic strength function (MSF), equation (33) of the large-scale magnetic fields of spiral galaxies at $z = 0$ in different SAMs, as indicated by the key. Each panel corresponds to a different galactic stellar mass interval, indicated in the top left of each frame. The points correspond to binned model results.

properties are different in galaxies of different masses and our results are presented for characteristic galactic mass ranges, where we have calculated the mass using only the stellar content.

The statistical properties of galactic magnetic fields are convenient to describe in terms of the number density of galaxies with a particular magnetic field strength per logarithmic interval of the filed strength; in the case of the large-scale magnetic field, this variable, referred to as the magnetic strength function (MSF), is defined as

$$\psi\left(\overline{B}\right) = \frac{\mathrm{d}n}{\mathrm{d}\,\log\overline{B}}\,. \tag{33}$$

4.1 The large-scale magnetic field

Fig. 3 shows the distribution of magnetic field strength, the MSF, for the large-scale field $\overline{B}$ in the local Universe ($z = 0$), each panel displaying a different galactic mass interval. The form of the MSF is sensitive to the galaxy formation model and, in each model, to the mass interval.

The typical magnetic field strengths are similar in the FON and BAU models, $0 \lesssim \log_{10}(\overline{B}/1\ \mu\mathrm{G}) \lesssim 1$. Except for the highest mass interval, the MSF of the LAG model is clearly bimodal, with the first peak in the interval 0.2-0.8 μG and the second close to the what is predicted by the other models.

Lower mass galaxies can have the strongest large-scale magnetic fields. Strong large-scale magnetic fields are increasingly suppressed with increasing mass and for galaxy masses $M_\star > 10^{10.25}\ \mathrm{M}_\odot$ there is a negligible number density of galaxies with large-scale magnetic fields stronger than ~ 10 μG. The reason for the suppression, discussed in more detail in Section 4.4, is the increase in the outflow speed in these galaxies, associated with their higher SFRs.

Another factor that affects Fig. 3 there is the overall decrease in the number density of galaxies with the galactic mass. This is expected from the shape of the galaxy stellar mass function of late-type galaxies, shown in Fig. 1. However, as it will be discussed later, the decrease is also intensified by the relatively small fraction of massive galaxies with active dynamos.

In Fig. 4, we show the fraction of galaxies with active large-scale dynamos (i.e. $|D| > |D_\mathrm{c}|$) as a function of galaxy mass at $z = 0$. The fraction of active dynamos in galaxies *decreases with mass* and all models predict that fewer than 40 per cent of galaxies have active dynamos for $M \gtrsim 10^{10}\ \mathrm{M}_\odot$. Fig. 5 provides a more detailed picture where the fraction of galaxies with a magnetic field strength exceeding 0.1, 1 and 10 μG is shown as a function of mass for each galaxy formation model separately.

The bimodal nature of the MSF of the LAG model in Fig. 3 is clarified by Fig. 6 where the MSF is shown separately for the central galaxies and their satellites: both the central galaxies and the satellites have unimodal MSFs but with maxima at different values of $\overline{B}$ in the LAG model. This is a consequence of the differences in the gas content of the satellite and central galaxy populations (see Section 4.4 for details).

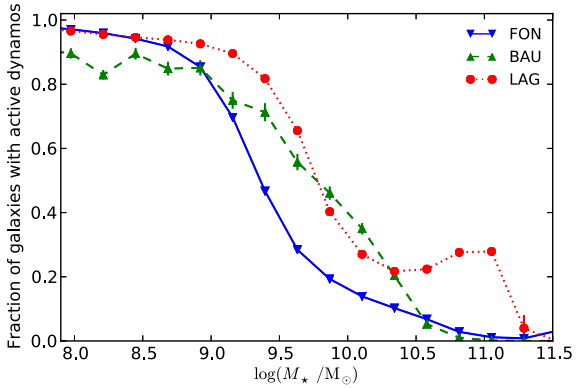

Figure 4. The fraction of galaxies with active dynamos (i.e. $|D| > |D_\mathrm{c}|$) at $z = 0$ as a function of galaxy mass in each model, as shown in the legend.

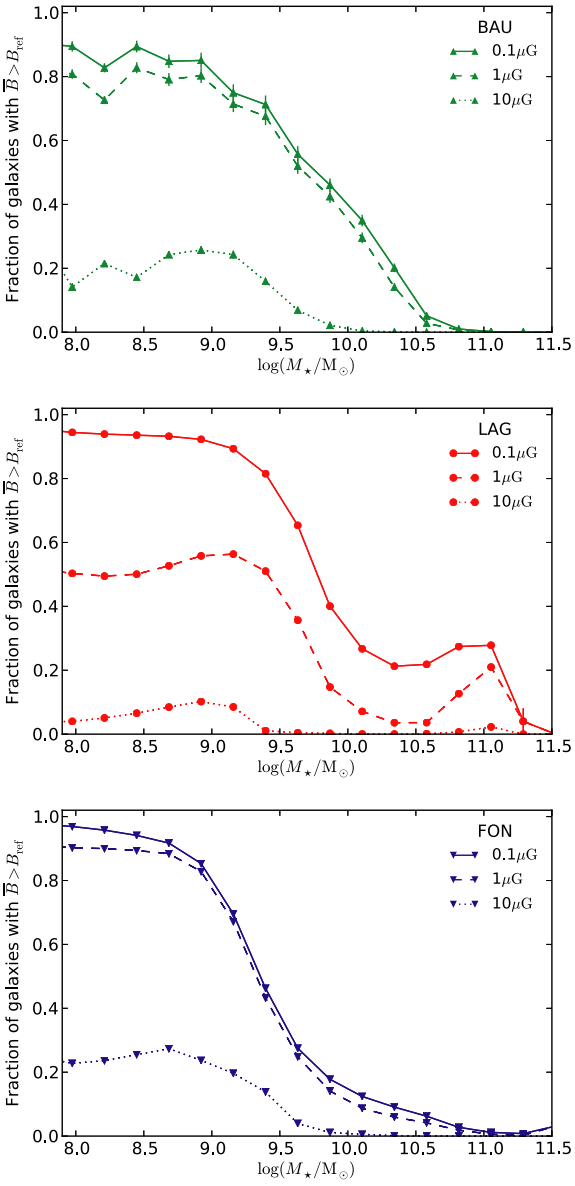

Figure 5. The fraction of galaxies with $\overline{B} > 0.1$, 1 and 10 μG at $z = 0$ as a function of the galaxy mass in each model, as specified in the legend.

4.2 The total magnetic field

Fig. 7 shows the MSF of the total magnetic field comprising both the large-scale and random parts, $B = (\overline{B}^2 + b^2)^{1/2}$; the MSF of the central galaxies is also shown with a dotted curve. The overall features of the large-scale magnetic field distributions of Fig. 3 can be seen in the total field as well. The most important differences occur at the two highest mass intervals where the MSF of the total magnetic field is significantly broader than the MSF of $\overline{B}$. At these masses, the small-scale magnetic fields dominate. This is consistent with the small fractions of active large-scale dynamos in these galaxies, as shown in Fig. 5.

In the LAG model, the tail of large-scale magnetic fields $\overline{B} \lesssim 0.1$ μG is concealed by stronger random magnetic fields, producing a cut-off at a mass-dependent minimum field strength. On the other hand, in the FON model, the opposite happens: there is a population galaxies (both satellites and central) with negligible large-scale magnetic field that contains random magnetic fields $b \lesssim 0.2$ μG. Such a change does not occur in the BAU model where the total magnetic field has a distribution not dissimilar to that of the large-scale field alone.

4.3 Evolution of galactic magnetic fields over cosmological time-scales

Fig. 8 shows the redshift evolution of the median value of the steady-state large-scale magnetic field in each galactic mass interval, as well as the 15th and 85th percentiles. Thus, at *a fixed mass interval*, the median of the large-scale magnetic field increases quasi-exponentially with redshift. The main reason for this increase are the larger interstellar gas densities that occur at higher redshifts. One must, however, bear in mind that Fig. 8 reflects changes in both magnetic field strength and galaxy mass with redshift.

The large-scale magnetic fields are expected to evolve on a time-scale of 10^8–10^9 yr (Beck et al. 1994; Shukurov 2007). On the one hand, the dynamo time-scale is shorter than the galactic evolution time, which allows us to use the steady-state strength of magnetic field in our estimates presuming that the dynamo action generates the large-scale magnetic field in a young galaxy and then adjusts itself instantaneously to the evolving galactic environment. This approximation is evidently acceptable in the inner parts of a galaxy where the rotational velocity shear is high and hence the dynamo time-scale is short. However, the effects of a finite dynamo time-scale can be significant in the outer parts of galaxies.

To illustrate these arguments, consider again the time-scale of the mean-field dynamo given by equation (20). Assuming, for the sake of illustration and by analogy with the Milky Way, that $h = 0.2$ kpc at $r = 1$ kpc and $\Omega = V_0/r$ with $V_0 = 200\,{\rm km\,s^{-1}}$, we obtain for the inner galaxy

$$\tau_{\rm MF} \simeq 20\,{\rm Myr}\left(\frac{r}{1\,{\rm kpc}}\right),$$

having adopted $D_{\rm c} \approx -8$ and $|D| \simeq 30 \gg |D_{\rm c}|$ at $r \simeq 1$ kpc. Thus, the e-folding time of the large-scale magnetic field can be as short as 20 Myr in the inner galaxy. With $h = 0.5$ kpc at $r = 10$ kpc, and adopting $D_{\rm c} - D = 4$ for illustration, we have $\tau_{\rm MF} \simeq 0.7$ Gyr in the outer galaxy. The effective large-scale seed magnetic field produced by the fluctuation dynamo is estimated by Beck et al. (1994) as $\overline{B}_{\rm s} = 10^{-3}$ μG; then the time required to amplify it to a strength $\overline{B} = 1$ μG is about $7\tau_{\rm MF}$. These estimates suggest that the inner few kiloparsecs of galactic discs would host microgauss-strong large-scale magnetic fields very soon after their formation. A galaxy formed at a redshift $z = 10$ would have its central kiloparsec magnetized with a large-scale magnetic field by $z \approx 8$, whereas a microgauss-strong magnetic field can build up via the local dynamo action by $z \approx 1$ at $r = 10$ kpc (see also Beck et al. 1994).

The above estimate is rather conservative since, due to the stronger dynamo action in the inner galaxy, the outer radius of the magnetized region increases approximately linearly in time at a speed $V_{\rm f} \simeq \sqrt{\gamma\eta}$ (Moss, Shukurov & Sokoloff 1998); this expansion can be described as the propagation of a magnetic front driven by the mean-field dynamo action. Taking $h = 0.3$ kpc as a representative value for the whole disc and $\eta = 10^{26}\,{\rm cm^2\,s^{-1}}$, we obtain $V_{\rm f} \simeq 6(r/1\,{\rm kpc})^{-1/2}\,{\rm km\,s^{-1}}$, and the front reaches $r = 10$ kpc in $t = \int_0^r {\rm d}r/V_{\rm f} \simeq 3.5$ Gyr. Thus, a magnetic front propagating outwards from the inner galaxy can produce a strong magnetic field in the outer galaxy by $z \simeq 1.5$, sooner than suggested by the above estimate of the local growth time at $r = 10$ kpc. Effectively, the propagating magnetic front provides a strong seed magnetic field

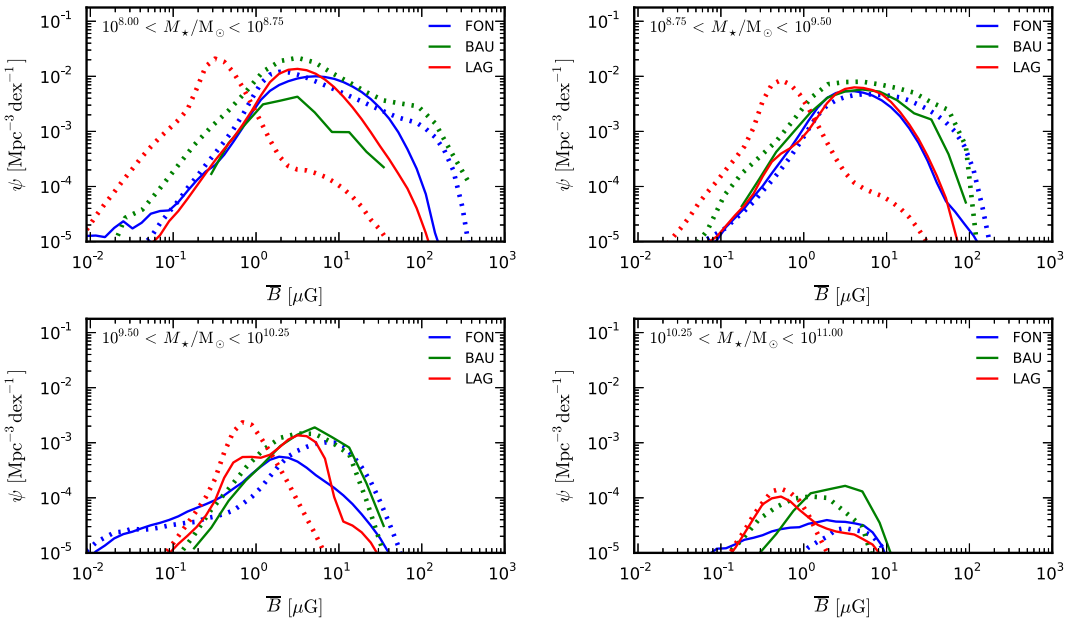

Figure 6. The distribution of large-scale magnetic field strengths at $z = 0$; each panel shows different galaxy stellar mass interval, as labelled. Dotted curves show the MSF associated with satellite galaxies and continuous lines show the MSF of central galaxies.

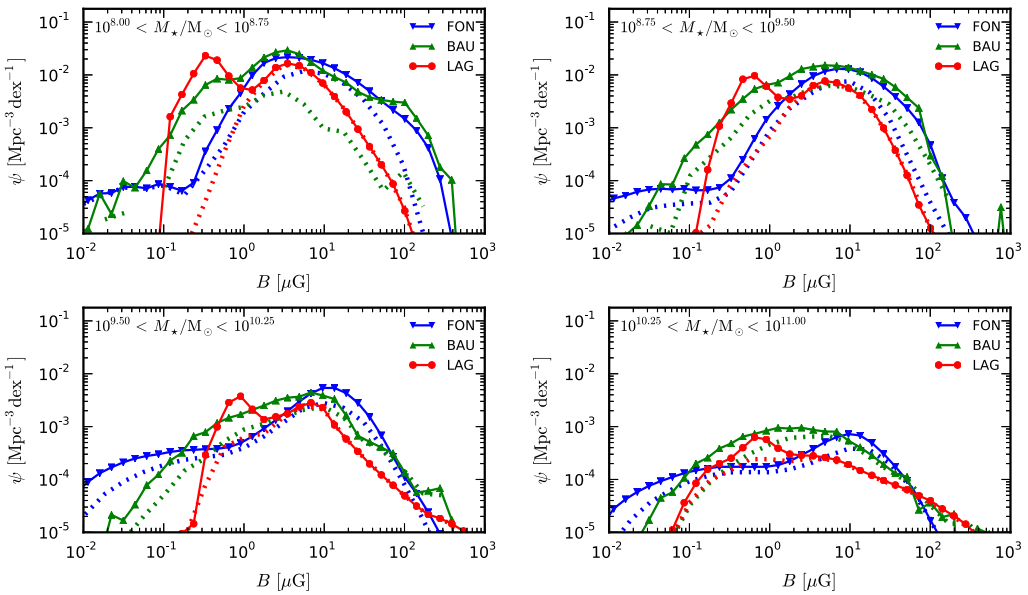

Figure 7. The distribution of the total magnetic field strength, $B = (\overline{B}^2 + b^2)^{1/2}$, in different galaxy stellar mass intervals at $z = 0$, as labelled in each panel. Dotted lines show the corresponding distributions for the central galaxies alone. Different colours are used to indicate different SAMs as specified in the legend.

for the local dynamo action thus leading to a faster build-up of the large-scale magnetic field.

We stress that turbulent magnetic fields can be produced on much shorter time-scales anywhere in the galaxy (Section 3.1).

These estimates of the redshift at which a spiral galaxy can develop a microgauss-strong large-scale magnetic field are somewhat higher than those of Arshakian et al. (2009, 2011) since these authors did not consider the fact that the dynamo time-scale is shorter in the inner galaxy: their estimates apply to the local dynamo action at $r \simeq 10$ kpc.

Since the dynamo model used here does not include the dynamo time-scales explicitly, assuming that they are shorter than the galactic evolution times, we only extend our results to $z = 2.5$. At this redshift, the outer radius of the part of the galactic disc occupied by the large-scale magnetic field of a microgauss strength is about 6 kpc, allowing for local dynamo action alone. Extension of the model to include evolutionary equations for magnetic field will be published elsewhere.

Figs 9–11 show the MSF at different redshifts for each galaxy formation model. Except for a shift towards higher values of $\overline{B}$,

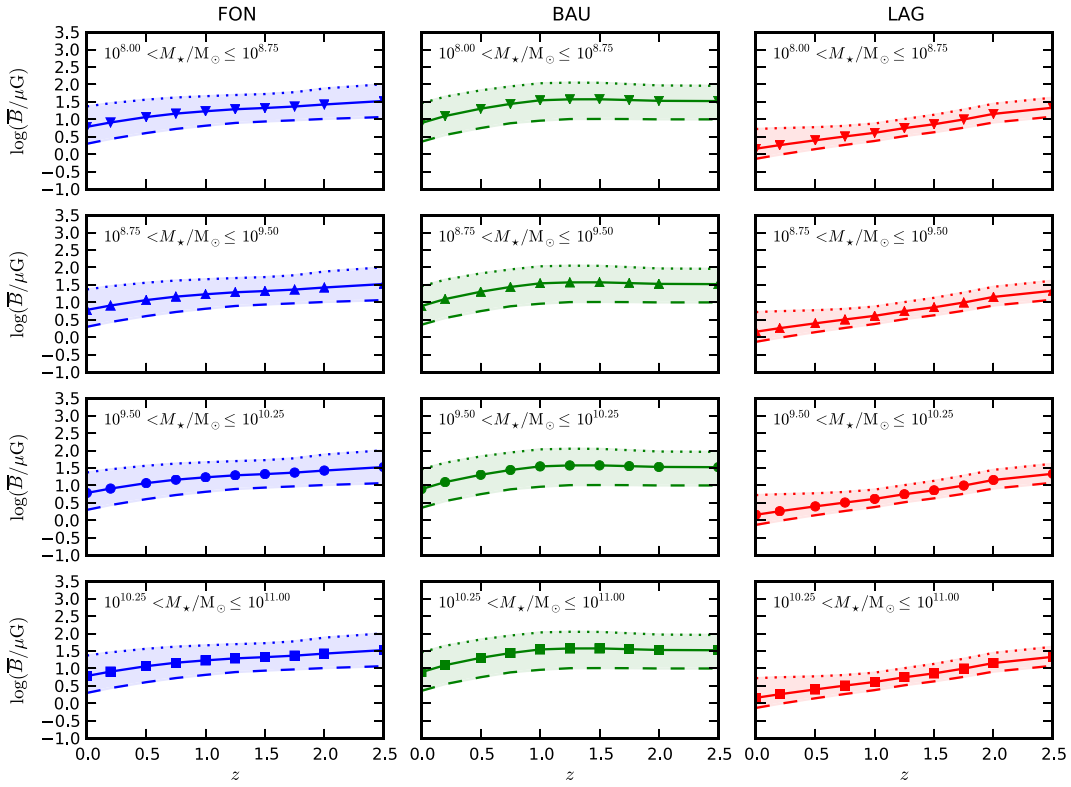

Figure 8. Redshift evolution of the large-scale magnetic field. The solid lines show the median field values. Dashed and dotted lines correspond to the 15th and 85th percentiles, respectively. Different columns correspond to different models (as indicated in the top row) and different rows show the results for different galaxy mass intervals (as indicated).

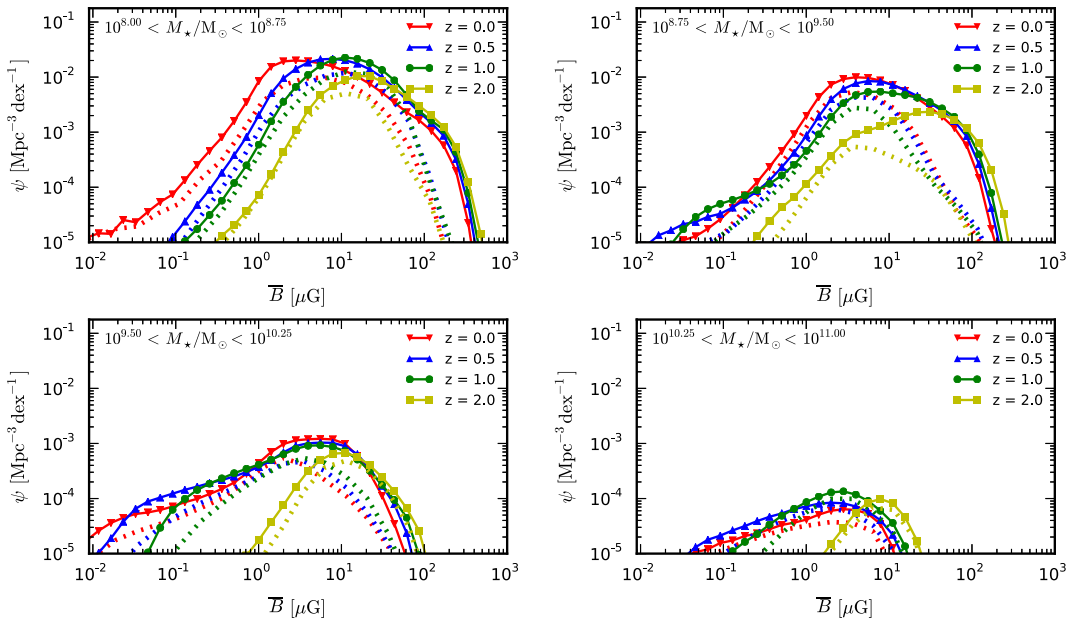

Figure 9. The evolution of the MSF in the case of the FON model. The dotted curves correspond the MSF of central galaxies. Different colours indicate the predictions for different redshifts as labelled.

there is not much variation in the shape of the MSF with redshift for the less massive galaxies.

In the same figures, dotted curves show the MSF of central galaxies alone, suggesting that there is no significant change in the relative contributions of the central and satellite galaxies to the MSFs.

4.4 Magnetic fields and the gas content of a galaxy

The form of the MSF is closely related to the gas content of galaxies. The gas density enters the reference magnetic field strength $B_{\rm eq}$ through equation (23). Moreover, the efficiency of magnetic helicity advection, quantified by R_u of equation (27), depends on the SFR,

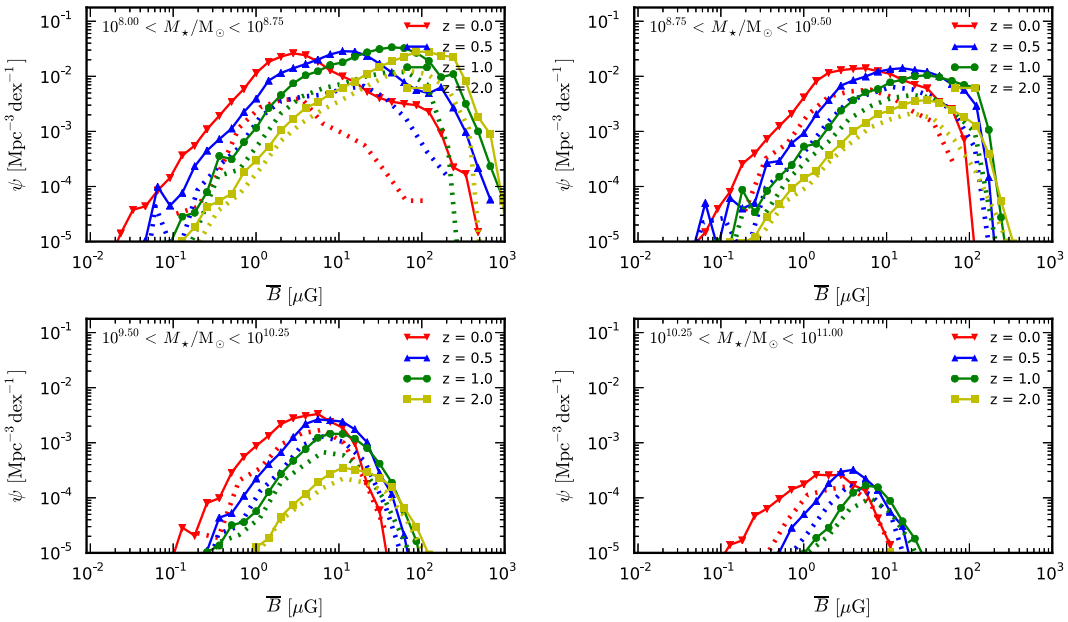

Figure 10. The evolution of the MSF for the BAU model. The dotted curves correspond the MSF of central galaxies. Different colours indicate the predictions for different redshifts as labelled.

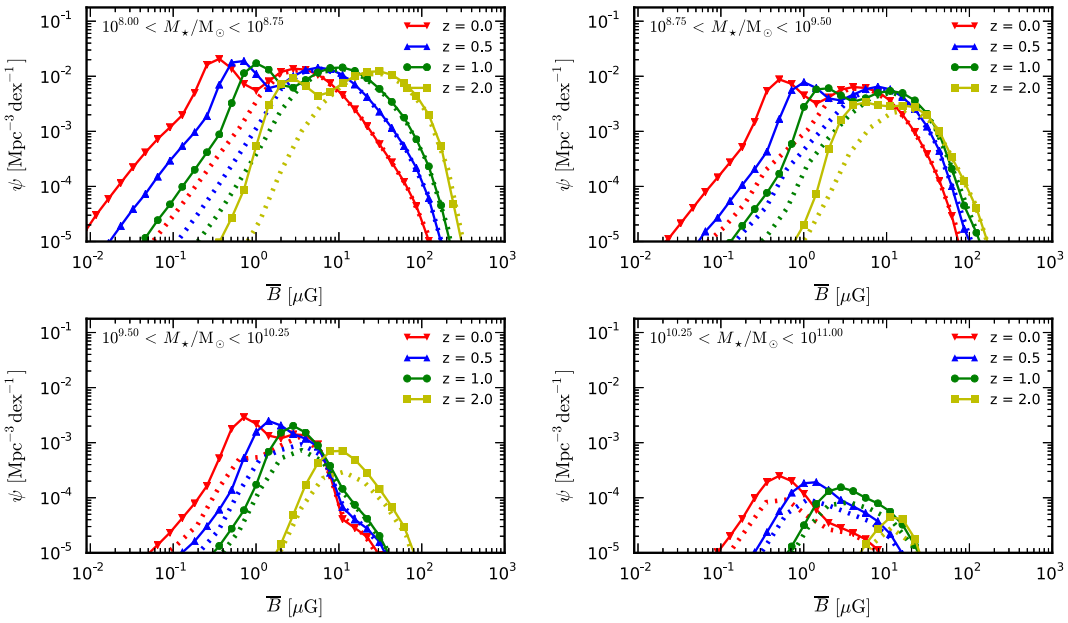

Figure 11. The evolution of the MSF for the LAG model. The dotted curves correspond the MSF of central galaxies. Different colours indicate the predictions for different redshifts as labelled.

which is controlled by the amount of cold gas in the galactic disc available to be converted into stars.

Equation (30) shows that galaxies with stronger star formation, and hence larger R_u, can have stronger large-scale magnetic fields. However, larger values of R_u also make the critical dynamo number higher, as shown by equation (29). As a result, there exists an SFR optimal for the mean-field dynamo action. In galaxies with large R_u the dynamo action is suppressed. Because of their higher SFRs, this affects massive galaxies especially strongly, systematically reducing, with the galactic mass, both the strength of their magnetic fields (as can be seen in the plots of the MSF) and the fraction of galaxies with active dynamos as shown in Fig. 4.

4.5 The importance of the ram-pressure stripping

An important consequence of the non-linear relationship between the gas content, star formation and the magnetic field strength is the difference between the MSFs of central and satellite galaxies shown in Fig. 6. Because of the loss of hot gas by the satellites due to ram-pressure stripping, both the gas density and SFR in them decrease leading to weaker outflows, thereby lowering $\overline{B}$. The effect is more evident for the LAG model because of the assumption of instantaneous ram-pressure stripping of the hot gas halo of the satellite (the so-called satellite starvation). For the FON model, the separation between the MSFs of satellite and central galaxies is

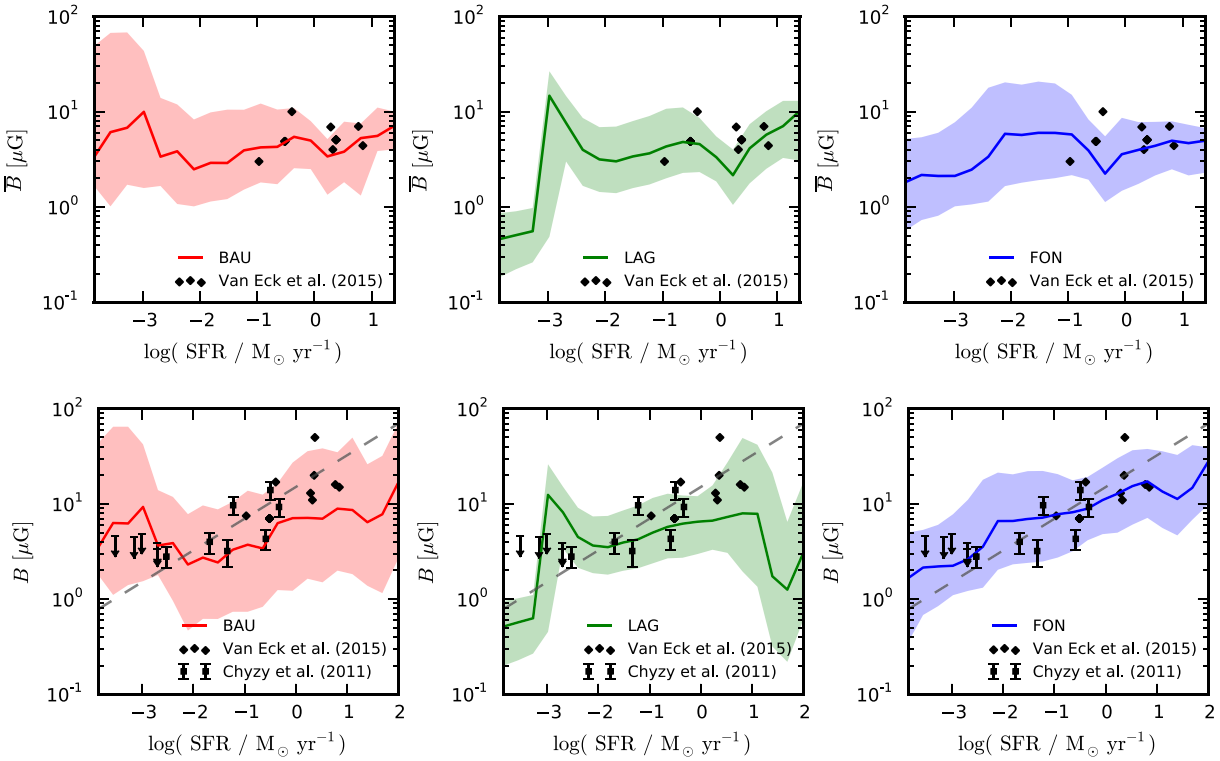

Figure 12. The dependence of the large-scale field strength, $\overline{B}$ (upper row), and total magnetic (lower row), B, on the star formation rate (SFR) predicted by each model. The solid lines show the median magnetic field values while the shaded areas show the range between the 15th and 85th percentiles. The square data points and triangles correspond, respectively, to the observed values and upper limits obtained by Chyży et al. (2011) for dwarf irregular galaxies in the Local Group. The diamond-shaped data points were calculated from the compilation made by Van Eck et al. (2015, their table 2): when the surface density of star formation, $\Sigma_{\rm SFR}$ was absent, we adopted the value corresponding to the innermost galactic radius; the total SFR was then obtained by integrating the surface density of SFR, $\Sigma_{\rm SFR}$, and the overall magnetic field was taken as the area-weighted average of the reported values. The dashed grey curve in the bottom row shows the relation $B \propto {\rm SFR}^{1/3}$ with an arbitrary choice of the intercept (see text).

smaller, reflecting the gradual ram-pressure stripping adopted in this model.

In the BAU model, despite the same efficiency of the ram-pressure stripping as in the LAG model, the MSF has a maximum at nearly the same positions for both the satellite and central galaxy populations. The reason is the star formation law adopted in this model, which leads to a higher SFR in galaxies with smaller circular velocity, as it follows from equation (1). The increase in SFR in lower mass galaxies leads to an increase in R_u, compensating the effects of starvation.

4.6 Magnetic field strength and star formation rate

The dependence of magnetic field strength on the SFR is due to an explicit dependence of the large-scale field strength (equation 30) on the outflow Reynolds number R_u defined in equation (27), with $v_{\rm ad}$ given in equations (18) and (19). In addition, the SFR is involved in the mean-field dynamo action through the dependence of the critical dynamo number on R_u in equation (29). With the galactic outflow model used here (Appendix B), the outflow speed is proportional to $L_{\rm SN}^{1/3}$, the energy supply rate from SNe in OB associations, and thus to ${\rm SFR}^{1/3}$. However, we then assume that all OB associations have the same energy supply rate, so that the outflow speed is proportional to the SFR. As a result, equation (30) predicts that $\overline{B} \propto {\rm SFR}^{1/2}$ in galaxies with a strong outflow (where $R_u > \pi^2 R_\kappa$), $\overline{B}$ is independent of the SFR if the outflow is weaker, and the dynamo action is suppressed completely by very strong outflows, such that $|D| < |D_{\rm c}|$.

The overall dependence of the total and large-scale magnetic field strengths on the SFR obtained in our model is shown in the bottom and top rows of Fig. 12, respectively. The large-scale magnetic field strength is roughly independent of the SFR and the model predictions are compatible with observations of nearby spiral galaxies compiled by Van Eck et al. (2015). The second row shows the variation of total magnetic field strength with the SFR. The model predictions are compatible with observations of both nearby spiral galaxies and Local Group dwarf irregular galaxies (Chyży et al. 2011). For comparison, we also show (the dashed grey curve) the frequently adopted power-law dependence $B \propto {\rm SFR}^m$ with $m \approx 1/3$. A power-law dependence is compatible with the predictions of the BAU and LAG over narrow SFR ranges and of the FON model over the whole SFR range.

When interpreting the lower row of Fig. 12, one ought to bear in mind that, since the total magnetic field is dominated by the random component and the turbulent velocity is fixed in our models (see Section 3.1), the emerging relation between the field strength and the SFR is a consequence of the non-linear relation between gas density and SFR and *not* of the dependence of the turbulent velocity on the SFR.

Schleicher & Beck (2013) argue that inverse Compton scattering of cosmic ray electrons can dominate their synchrotron losses from redshift $z \approx 3$ upwards, thus affecting the observability of galactic magnetic fields at high redshift. We note, however, that these authors

use interstellar gas parameters obtained by Thompson, Quataert & Murray (2005) for starburst galaxies with the surface density of star formation $\Sigma_\star \simeq 10^3\ \mathrm{M_\odot\,kpc^{-2}\,yr^{-1}}$, where vertical support against gravity is provided by radiation pressure. However, they apply this model to galaxies with surface density of SFR of order $\Sigma_\star = 0.1\ \mathrm{M_\odot\,kpc^{-2}\,yr^{-1}}$ where the properties of the interstellar gas are rather different. Perhaps more importantly, Schleicher & Beck (2013) employ a simple relation $B \propto \Sigma_\star^{1/3}$ for the total magnetic field strength (dominated by the random magnetic field). As discussed above, any relation of B to $\Sigma_\star$ is likely to be more complicated and can definitely be different in galaxies of different masses and different SFRs. As discussed in Section 2.2.1, the main reason for this is that the turbulent speed in the interstellar gas is self-regulated to be comparable to the sound speed (if the energy supply is high enough), because supersonic turbulence quickly dissipates the excess kinetic energy into heat thus increasing the speed of sound. In galaxies with strong star formation, a progressively larger part of the energy supplied by SNe and stellar winds is channelled into galactic outflows rather than turbulence. Since the hot gas leaves the disc at time-scales shorter than even the fluctuation dynamo time, both large-scale and random magnetic fields of galactic discs are generated in the warm gas where the speed of sound is of order $10\,\mathrm{km\,s^{-1}}$. This strongly non-linear effect seems to preclude any universal dependence of the turbulent speed and magnetic field strength on the SFR applicable beyond relatively narrow ranges of galactic mass and SFR. This makes the conclusions of Schleicher & Beck (2013) questionable. The dependence of galactic magnetic field strength on SFR is usually discussed in connection with the radio–far-infrared correlation (e.g. Yun, Reddy & Condon 2001, and references therein), where this dependence is just one element of a complex physical system. It is not our intention to discuss or explain that correlation, even though our conclusions are relevant to the discussions of its nature.

Since galaxy mergers are instantaneous in SAMs, we cannot include any effects of the mergers on galactic magnetic fields. However, the starburst produced by a merger is a part of the SAMs; both large-scale and turbulent magnetic fields are enhanced during a starburst in our model. The effects of galaxy mergers on the mean-field dynamo can be non-trivial (Drzazga et al. 2011; Geng et al. 2012; Kotarba et al. 2011), but their inclusion would require a more detailed model of both galaxy formation and dynamo action that those used here.

4.7 Advection and diffusion of magnetic helicity

Table 2 shows that most galaxies with an active mean-field dynamo have $R_u < \pi$. Thus, the strength of the large-scale magnetic field, given in equation (30), is dominated by the diffusion of magnetic helicity for the value of R_κ used, $R_\kappa = 0.3$. This reduces significantly the effect of galactic outflows on the mean-field dynamo action.

Table 2. Fraction of galaxies with active dynamos and $R_u < \pi$ in the galaxy formation models explored.

Mass interval $\log M_\star/\mathrm{M_\odot}$	LAG per cent	BAU per cent	FON per cent
8.00–8.75	85	88	93
8.75–9.50	89	89	95
9.50–10.25	92	87	92
10.25–11.00	92	89	90

Equation (30) has been derived by Chamandy et al. (2014) with the diffusive flux of the magnetic helicity α_m (proportional to the mean current helicity of the random magnetic field, $\boldsymbol{b}\cdot\nabla\times\boldsymbol{b}$) obtained assuming that the scaleheight of α_m is equal to that of the ionized gas. Almost nothing is known about the spatial distribution of the mean current helicity even from numerical simulations, not to mention observations. The numerical simulations of Gressel et al. (2008, see also Gressel, Bendre & Elstner 2013) suggest that the scale of the total α-effect across the gas layer can be significantly larger (at about 1 kpc in the solar vicinity of the Milky Way) than the gas scaleheight, perhaps due to the contribution of α_m. If this is the case, the value of R_κ is strongly overestimated. Then the dynamo model underestimates the role of galactic outflows and, hence, star formation on the large-scale magnetic field. The relative roles of galactic outflows and diffusion in the non-linear mean-field dynamos requires further careful study under realistic conditions for spiral galaxies.

5 SUMMARY AND CONCLUSIONS

By coupling a non-linear mean-field dynamo model with three well-established SAMs of galaxy formation, we have developed a framework to predict the strength of large-scale (global) and small-scale (turbulent) magnetic fields in evolving spiral galaxies from the time when their bulge to disc mass ratio reduces below 1/2 and they are classified as late types. We present our results for various galactic stellar mass ranges selected according to the physical properties of the galaxies and we consider the evolution of galactic magnetic fields with redshift. Our main assumption is that the steady-state strength of the magnetic field is established instantaneously as the host galaxy evolves. This assumption is not questionable for the turbulent magnetic fields as the time-scale of the fluctuation dynamo producing them can be as short as 10 Myr. The time-scale of the large-scale (mean-field) dynamo is longer at about a few Gyr in the main part of a spiral galaxy but can be two orders of magnitude shorter in the inner galaxy. This time-scale is at least marginally shorter than the galactic evolution time, which justifies our assumption.

We find that the choice of the galaxy formation model strongly affects the number density of galaxies that host a large-scale magnetic field of a given strength (called the MSF in the text) in most mass ranges. In other words, the probability distribution of the strength of the large-scale magnetic field in a representative sample of galaxies is sensitive to the galaxy formation model. We discuss how the shape of the MSF is related to the physical processes affecting the dynamo action and how these depend on the galaxy formation model. In particular, the ram-pressure stripping of the gas in the haloes of satellite galaxies results in quite different typical field strengths in satellites and their central galaxies, which can lead to a pronounced bimodality of the MSF. Our experience thus demonstrates the possibility of using observations of galactic magnetic fields to constrain galaxy formation models.

Our results are also relevant to planning observational studies of galactic magnetism at high redshifts. Galaxies that host a large-scale magnetic field can produce a signal in polarized synchrotron emission, even when they are unresolved: the degree of polarization depends on the orientation of the galactic disc to the line of sight and the degree of order in the magnetic field (Stil et al. 2009). Thus, radio continuum surveys that cover both total and polarized synchrotron emission, using the Square Kilometre Array and other radio telescopes, will be able to produce statistical distributions of fractional polarization for the local universe and for different

redshifts, that can be directly compared to our (or similar) models. This data will provide a new window through which to test both galaxy evolution models and theories of magnetic field evolution in galaxies. For example, all of the galaxy formation models considered here predict that less than 50 per cent of the spiral galaxies with stellar mass greater than 10^{10} $M_{\odot}$ should host large-scale magnetic fields greater than 1 μG in strength. Similar statements are made for other mass ranges in the main text and illustrated in Fig. 5.

Our results suggest that the strength of the large-scale galactic magnetic field increases nearly exponentially with redshift in all mass ranges. This does not, however, mean that the magnetic field in an individual galaxy evolves exponentially because individual galaxies migrate between the mass ranges and, more importantly, individual galaxies become dynamo active at different stages of their evolution (even within a relatively narrow mass interval) because of different individual merger trees.

Our approach can be improved in several ways. Most importantly, by allowing for a finite magnitude of the dynamo time-scale, we shall be able to include detailed evolution of magnetic field allowing us to predict with confidence the appearance of individual galaxies in the radio range and to assess the importance of magnetic field effects on star formation in evolving galaxies, and to trace back a given magnetic configuration to earlier stages.

ACKNOWLEDGEMENTS

LFSR thanks Durham University for the hospitality during his visit and acknowledges support from the European Commission's Framework Programme 7, through the Marie Curie International Research Staff Exchange Scheme LACEGAL (PIRSES-GA-2010-269264) and support from the Brazilian Agency CNPq (202466/2011-6) during the initial part of this work. LFSR, AS and AF have been supported by the Leverhulme Trust (grant RPG-097) and STFC (grant ST/L005549/1). CMB acknowledges support from the STFC grant ST/L00075X/1. This work used the DiRAC Data Centric system at Durham University, operated by the Institute for Computational Cosmology on behalf of the STFC DiRAC HPC Facility (www.dirac.ac.uk). This equipment was funded by BIS National E-infrastructure capital grant ST/K00042X/1, STFC capital grant ST/H008519/1 and STFC DiRAC Operations grant ST/K003267/1 and Durham University. DiRAC is a part of the National E-Infrastructure. We are grateful to the referee for useful comments and suggestions.

REFERENCES

Arshakian T. G., Beck R., Krause M., Sokoloff D., 2009, A&A, 494, 21
Arshakian T. G., Stepanov R., Beck R., Krause M., Sokoloff D., 2011, Astron. Nachr., 332, 524
Baugh C. M., 2006, Rep. Prog. Phys., 69, 3101
Baugh C. M., Lacey C. G., Frenk C. S., Granato G. L., Silva L., Bressan A., Benson A. J., Cole S., 2005, MNRAS, 356, 1191
Beck R., Wielebinski R., 2013, in Oswalt T. D., Gilmore G., eds, Planets, Stars and Stellar Systems. Volume 5: Galactic Structure and Stellar Populations. Springer, Netherlands, p. 641
Beck R., Poezd A. D., Shukurov A., Sokoloff D. D., 1994, A&A, 289, 94
Beck R., Brandenburg A., Moss D., Shukurov A., Sokoloff D., 1996, ARA&A, 34, 155
Benson A. J., 2010, Phys. Rep., 495, 33
Berezinskii V. S., Bulanov S. V., Dogiel V. A., Ptuskin V. S., 1990, in Ginzburg V. L., ed., Astrophysics of Cosmic Rays. North-Holland, Amsterdam
Bhat P., Subramanian K., 2013, MNRAS, 429, 2469
Birnboim Y., 2009, ApJ, 702, L101
Birnboim Y., Balberg S., Teyssier R., 2015, MNRAS, 447, 3678
Blitz L., Rosolowsky E., 2006, ApJ, 650, 933
Bloemen J. B. G. M., 1987, ApJ, 322, 694
Booth C. M., Agertz O., Kravtsov A. V., Gnedin N. Y., 2013, ApJ, 777, L16
Boulares A., Cox D. P., 1990, ApJ, 365, 544
Bower R. G., Benson A. J., Malbon R., Helly J. C., Frenk C. S., Baugh C. M., Cole S., Lacey C. G., 2006, MNRAS, 370, 645
Brandenburg A., Subramanian K., 2005, Phys. Rep., 417, 1
Breitschwerdt D., Komossa S., 2000, Ap&SS, 272, 3
Chamandy L., Shukurov A., Subramanian K., Stoker K., 2014, MNRAS, 443, 1867
Chyży K. T., Weżgowiec M., Beck R., Bomans D. J., 2011, A&A, 529, A94
Cole S., Lacey C. G., Baugh C. M., Frenk C. S., 2000, MNRAS, 319, 168
Crutcher R. M., 2012, ARA&A, 50, 29
de Avillez M. A., Breitschwerdt D., 2004, A&A, 425, 899
Del Sordo F., Guerrero G., Brandenburg A., 2013, MNRAS, 429, 1686
Dib S., Bell E., Burkert A., 2006, ApJ, 638, 797
Drzazga R. T., Chyży K. T., Jurusik W., Wiórkiewicz K., 2011, A&A, 533, A22
Durrer R., Neronov A., 2013, A&AR, 21, 62
Dutton A. A. et al., 2011, MNRAS, 416, 322
Efstathiou G., Lake G., Negroponte J., 1982, MNRAS, 199, 1069
Elmegreen B. G., Scalo J., 2004, ARA&A, 42, 211
Everett J. E., Zweibel E. G., Benjamin R. A., McCammon D., Rocks L., Gallagher J. S., III, 2008, ApJ, 674, 258
Fanidakis N., Baugh C. M., Benson A. J., Bower R. G., Cole S., Done C., Frenk C. S., 2011, MNRAS, 410, 53
Fanidakis N. et al., 2012, MNRAS, 419, 2797
Federrath C., Chabrier G., Schober J., Banerjee R., Klessen R. S., Schleicher D. R. G., 2011, Phys. Rev. Lett., 107, 114504
Ferriere K. M., Mac Low M.-M., Zweibel E. G., 1991, ApJ, 375, 239
Fletcher A., Shukurov A., 2001, MNRAS, 325, 312
Fletcher A., Berkhuijsen E. M., Beck R., Shukurov A., 2004, A&A, 414, 53
Fletcher A., Beck R., Shukurov A., Berkhuijsen E. M., Horellou C., 2011, MNRAS, 412, 2396
Font A. S. et al., 2008, MNRAS, 389, 1619
Gaensler B. M., Beck R., Feretti L., 2004, New Astron. Rev., 48, 1003
Geng A., Kotarba H., Bürzle F., Dolag K., Stasyszyn F., Beck A., Nielaba P., 2012, MNRAS, 419, 3571
Gent F. A., Shukurov A., Sarson G. R., Fletcher A., Mantere M. J., 2013a, MNRAS, 430, L40
Gent F. A., Shukurov A., Fletcher A., Sarson G. R., Mantere M. J., 2013b, MNRAS, 432, 1396
González J. E., Lacey C. G., Baugh C. M., Frenk C. S., Benson A. J., 2009, MNRAS, 397, 1254
Gressel O., Ziegler U., Elstner D., Rüdiger G., 2008, Astron. Nachr., 329, 619
Gressel O., Bendre A., Elstner D., 2013, MNRAS, 429, 967
Hanayama H., Tomisaka K., 2006, ApJ, 641, 905
Hanayama H., Takahashi K., Kotake K., Oguri M., Ichiki K., Ohno H., 2005, ApJ, 633, 941
Haugen N. E. L., Brandenburg A., Mee A. J., 2004, MNRAS, 353, 947
Heiles C., 1987, ApJ, 315, 555
Ji Y., Cole L., Bushby P., Shukurov A., 2014, Geophys. Astrophys. Fluid Dyn., 108, 568
Kazantsev A. P., Ruzmaikin A. A., Sokolov D. D., 1985, Z. Eksp. Teor. Fiz., 88, 487
Kennicutt R. C., Jr, 1983, ApJ, 272, 54
Kleeorin N., Moss D., Rogachevskii I., Sokoloff D., 2000, A&A, 361, L5
Kleeorin N., Moss D., Rogachevskii I., Sokoloff D., 2002, A&A, 387, 453
Kleeorin N., Moss D., Rogachevskii I., Sokoloff D., 2003, A&A, 400, 9
Korpi M. J., Brandenburg A., Shukurov A., Tuominen I., 1999, A&A, 350, 230
Kotarba H., Lesch H., Dolag K., Naab T., Johansson P. H., Donnert J., Stasyszyn F. A., 2011, MNRAS, 415, 3189
Kulsrud R. M., Cen R., Ostriker J. P., Ryu D., 1997, ApJ, 480, 481

Lacey C. G., Baugh C. M., Frenk C. S., Benson A. J., 2011, MNRAS, 412, 1828
Lagos C. D. P., Lacey C. G., Baugh C. M., Bower R. G., Benson A. J., 2011a, MNRAS, 416, 1566
Lagos C. D. P., Baugh C. M., Lacey C. G., Benson A. J., Kim H.-S., Power C., 2011b, MNRAS, 418, 1649
Lagos C. D. P., Bayet E., Baugh C. M., Lacey C. G., Bell T. A., Fanidakis N., Geach J. E., 2012, MNRAS, 426, 2142
Lagos C. d. P., Lacey C. G., Baugh C. M., 2013, MNRAS, 436, 1787
Mac Low M.-M., 2009, Rev. Mex. Astron. Astrofis, 36, 121
Mac Low M.-M., Klessen R. S., 2004, Rev. Mod. Phys., 76, 125
Mac Low M.-M., McCray R., 1988, ApJ, 324, 776
McCarthy I. G., Frenk C. S., Font A. S., Lacey C. G., Bower R. G., Mitchell N. L., Balogh M. L., Theuns T., 2008, MNRAS, 383, 593
McCourt M., O'Leary R. M., Madigan A.-M., Quataert E., 2015, MNRAS, 449, 2
Mee A. J., Brandenburg A., 2006, MNRAS, 370, 415
Mishustin I. N., Ruzmaĭkin A. A., 1972, Sov. J. Exp. Theor. Phys., 34, 233
Mitra D., Candelaresi S., Chatterjee P., Tavakol R., Brandenburg A., 2010, Astron. Nachr., 331, 130
Moffatt H. K., 1978, Magnetic Field Generation in Electrically Conducting Fluids. Cambridge Univ. Press, Cambridge
Moss D., Shukurov A., 1996, MNRAS, 279, 229
Moss D., Shukurov A., Sokoloff D., 1998, Geophys. Astrophys. Fluid Dyn., 89, 285
Orsi A., Lacey C. G., Baugh C. M., Infante L., 2008, MNRAS, 391, 1589
Pakmor R., Marinacci F., Springel V., 2014, ApJ, 783, L20
Parker E. N., 1979, Cosmical Magnetic Fields: Their Origin and their Activity. Clarendon Press, Oxford p. 858
Peters T., Banerjee R., Klessen R. S., Mac Low M.-M., 2011, ApJ, 729, 72
Putman M. E., Peek J. E. G., Joung M. R., 2012, ARA&A, 50, 491
Rodrigues L. F. S., de Souza R. S., Opher R., 2010, MNRAS, 406, 482
Ruzmaikin A. A., Shukurov A. M., Sokoloff D. D., 1988, Magnetic Fields of Galaxies. Kluwer, Dordrecht
Scalo J., Elmegreen B. G., 2004, ARA&A, 42, 275
Schekochihin A. A., Cowley S. C., Hammett G. W., Maron J. L., McWilliams J. C., 2002a, New J. Phys., 4, 84
Schekochihin A., Cowley S., Maron J., Malyshkin L., 2002b, Phys. Rev. E, 65, 016305
Schleicher D. R. G., Beck R., 2013, A&A, 556, A142
Schleicher D. R. G., Banerjee R., Sur S., Arshakian T. G., Klessen R. S., Beck R., Spaans M., 2010, A&A, 522, A115
Seifried D., Banerjee R., Schleicher D., 2014, MNRAS, 440, 24
Shukurov A., 2007, in Dormy E., Soward A. M., eds, Mathematical Aspects of Natural Dynamos. CRC Press, Boca Raton, FL, p. 319
Shukurov A., Sarson G. R., Nordlund Å., Gudiksen B., Brandenburg A., 2004, Ap&SS, 289, 319
Shukurov A., Sokoloff D., Subramanian K., Brandenburg A., 2006, A&A, 448, L33
Springel V. et al., 2005, Nature, 435, 629
Stil J. M., Krause M., Beck R., Taylor A. R., 2009, ApJ, 693, 1392
Subramanian K., 1999, Phys. Rev. Lett., 83, 2957
Subramanian K., Shukurov A., Haugen N. E. L., 2006, MNRAS, 366, 1437
Sur S., Shukurov A., Subramanian K., 2007, MNRAS, 377, 874
Sur S., Federrath C., Schleicher D. R. G., Banerjee R., Klessen R. S., 2012, MNRAS, 423, 3148
Tamburro D., Rix H.-W., Leroy A. K., Mac Low M.-M., Walter F., Kennicutt R. C., Brinks E., de Blok W. J. G., 2009, AJ, 137, 4424
Tenorio-Tagle G., Bodenheimer P., 1988, ARA&A, 26, 145
Thompson T. A., Quataert E., Murray N., 2005, ApJ, 630, 167
Uhlig M., Pfrommer C., Sharma M., Nath B. B., Enßlin T. A., Springel V., 2012, MNRAS, 423, 2374
Van Eck C. L., Brown J. C., Shukurov A., Fletcher A., 2015, ApJ, 799, 35
Veilleux S., Cecil G., Bland-Hawthorn J., 2005, ARA&A, 43, 769
Wang P., Abel T., 2009, ApJ, 696, 96
Wilkin S. L., Barenghi C. F., Shukurov A., 2007, Phys. Rev. Lett., 99, 134501
Yun M. S., Reddy N. A., Condon J. J., 2001, ApJ, 554, 803
Zeldovich Y. B., Ruzmaikin A. A., Sokoloff D. D., 1983, Magnetic Fields in Astrophysics. Gordon and Breach, New York
Zeldovich Y. B., Ruzmaikin A. A., Sokoloff D. D., 1990, The Almighty Chance. World Scientific, Singapore

APPENDIX A: THE SCALEHEIGHT OF A PRESSURE-SUPPORTED THIN DISC

GALFORM assumes that the stars and gas in galaxy discs have an exponential radial profile of the stellar surface density,

$$\Sigma_{\star/\mathrm{g}}(r) = \frac{M_{\star/\mathrm{g}}}{2\pi r_\mathrm{s}^2} \mathrm{e}^{-r/r_\mathrm{s}}\,, \tag{A1}$$

where r_s is the scalelength and this is assumed to be the same for stars and gas.

Under the assumption of hydrostatic equilibrium in the z-direction, one obtains (using cylindrical coordinates) the following expression for the gas pressure, P,

$$\frac{\partial}{\partial z}\left(\frac{1}{\rho_\mathrm{g}}\frac{\partial P}{\partial z}\right) = 4\pi G\rho_\mathrm{t}\,, \tag{A2}$$

where ρ_t is the total gravitating mass density. Defining the surface densities

$$\Sigma(R,z) = 2\int_0^z \rho(R,z)\,\mathrm{d}z\,, \qquad \frac{\partial\Sigma}{\partial z} = 2\rho(R,z)\,, \tag{A3}$$

which is related to the total surface density through $\Sigma(R) = \lim_{z\to\infty}\Sigma(R,z)$ and using equation (A2), we obtain

$$\frac{\partial P}{\partial z} = \pi G\Sigma_\mathrm{t}\frac{\partial\Sigma_\mathrm{g}}{\partial z}\,. \tag{A4}$$

Since stars and gas are assumed to be distributed similarly, we have $\Sigma_\mathrm{g} = k\Sigma_\mathrm{t}$ with k a constant at a given time, which leads to

$$\Sigma_\mathrm{t}\frac{\partial\Sigma_\mathrm{g}}{\partial z} = \frac{1}{2}k\frac{\partial\Sigma_\mathrm{g}^2}{\partial z}\,.$$

Then, integrating equation (A4), gas pressure follows as

$$P = \frac{\pi}{2}G\Sigma_\mathrm{g}(\Sigma_\mathrm{g}+\Sigma_\star)\,. \tag{A5}$$

On the other hand,

$$P = \frac{\alpha}{3}v_0^2\rho\,, \tag{A6}$$

where α (>1) allows for various contributions to the interstellar gas pressure: thermal, turbulent and from cosmic rays and magnetic fields.

The scaleheight is obtained by combining equations (A1), (A5), (A6) and $\rho \approx \Sigma/h$, i.e. assuming weak vertical density variations:

$$h(r) = \frac{\alpha v_0^2 r_\mathrm{s}^2}{G(M_\star + M_\mathrm{gas})}\mathrm{e}^{r/r_\mathrm{s}}\,. \tag{A7}$$

APPENDIX B: GALACTIC OUTFLOWS DRIVEN BY SUPERNOVAE

We follow equation (2) from Mac Low & McCray (1988) for the radius, R_sb, of a superbubble produced by an OB association,

$$R_\mathrm{sb} = 267\,\mathrm{pc}\left(\frac{L_{38}\,t_7^3}{n_0}\right)^{1/5}\,,$$

where L_{38} is the mechanical luminosity in the unit of $10^{38}\,\mathrm{erg\,s^{-1}}$, t_7 is time in the unit of 10^7 yr and n_0 is the number density of the ambient gas. The superbubble expands at the speed

$$\dot{R}_{\rm sb} = 15.7\,\mathrm{km\,s^{-1}} L_{38}^{1/5} n_0^{-1/5} t_7^{-2/5}.$$

Mac Low & McCray (1988) find that the superbubble breaks out from the disc when $R \approx 2h$. This can be used with the previous equations to obtain the superbubble age at the break-out,

$$t_7^{-2/5} = \left(\frac{n_0}{L_3 8}\right)^{-2/15} h_{134}^{-2/3},$$

where $h_{134} = h/134\,\mathrm{pc}$. Therefore, the velocity of the shock front produced by the superbubble at the break-out is

$$\begin{aligned} v_{\rm sh} &= \dot{R}_{\rm sb}\big|_{R_{\rm sb}=2h} \\ &= 4\ \mathrm{km\,s^{-1}} \left(\frac{L_{\rm SN}}{10^{38}\,\mathrm{ergs^{-1}}}\right)^{1/3} \left(\frac{n_0}{1\,\mathrm{cm^{-3}}}\right)^{-1/3} \left(\frac{h}{1\,\mathrm{kpc}}\right)^{-2/3}, \end{aligned}$$

and assuming $L_{38} = 1$, one arrives at equation (13).

This paper has been typeset from a TEX/LATEX file prepared by the author.